Methylglyoxal Effects in Cell Therapy for Myocardial Infarction

by

Mayte Lorena Gonzalez Gomez

This thesis is submitted to the

Faculty of Graduate and Postdoctoral Studies

as a partial fulfillment of the requirements for the

M.Sc. program in Cellular and Molecular Medicine

Department of Cellular and Molecular Medicine

Faculty of Medicine

University of Ottawa

August 21st, 2018

i. Acknowledgments

Undertaking this M.Sc. in Canada has been a truly life-changing experience for me and it would not have been possible without the support and guidance from many people. For this reason, I want to express my thankfulness for their contribution in the elaboration of the present work.

I am forever grateful to my supervisor, Dr. Erik Suuronen, for accepting me as part of his research team. I will never forget how I got a reply briefly after sending my first email at 5:00 am, and all his patience while explaining the ongoing projects of the lab by phone. Thank you so much for your dedication, patience and understanding during all the stages of this thesis.

I owe a great deal of gratitude to the members of my thesis advisory committee at the University of Ottawa: Dr. Catherine Tsilfidis and Dr. David Allan.

I would also like to express a profound gratitude to Rick Seymour, Vivian Franklin, and the animal care team from the University of Ottawa Heart Institute.

Special mention is deserved to Brian McNeill who provided me with the training, active guidance and valuable suggestions throughout this study.

Definitive for the completion of this project was the pleasant atmosphere that I found at the UOHI thanks to many current and former lab members. I can leave happy knowing that not only did I find superb labmates, but also great friends. Thank you so much Danielle, Çağla, and Veronika for guiding me, teaching me and encouraging me, always for the best. Thank you as well for all those necessary coffee breaks.

I am also grateful for all the friends that I made during these two years in Canada. You are now a second family and without you, I would have missed thousands of opportunities to fully enjoy this experience.

On a different note, I also acknowledge the Science and Technology Council of Mexico (Consejo Nacional de Ciencia y Tecnología, CONACyT) for its financial support throughout my master's in science program.

And last but no least, I heartily wish to express my deepest gratitude to my friends and especially to my family in Mexico. Thanks, mamá and papá for always supporting me in my adventures, thank you for not stop believing in me. This achievement is for you.

ii. Abstract

Methylglyoxal (MG), a highly reactive dicarbonyl accumulates after myocardial infarction (MI), causing adverse remodelling and cardiac dysfunction. We hypothesized that therapy using bone marrow cells (BMCs) overexpressing glyoxalase1 (Glo1), the main enzyme that metabolizes MG, injected into mouse MI model would translate into better survival of transplanted cells and improve their therapeutic effect.

We found that *Glo*1 expression is significantly reduced at 7 days post-MI. Glo1 BMCs exposed to MG *in vitro* displayed greater angiogenic potential and reduced reactive oxygen species production compared to wild type (WT) BMCs. However, in the mouse MI model, Glo1 BMCs did not improve cardiac function or vascularity or reduce scar formation compared to WT BMCs and saline treatments.

In conclusion, Glo1 overexpression in BMCs does not confer superior therapeutic efficacy for treating MI under the conditions tested.

iii. Table of contents

1. List of tables and figures

iii. List of abbreviations

S.I. (Système International d'Unités) abbreviations for units and standard notations for chemical elements, formulae and chemical abbreviations are used in this work. Other abbreviations are listed below:

Angiotensin-converting enzyme	**ACE**
Advanced glycation end-products	**AGEs**
Adenosine triphosphate	**ATP**
Bone marrow	**BM**
Bone marrow cells	**BMCs**
Cluster of differentiation 31	**CD31**
Chloromethyl benzoyl amino tetramethylrhodamine	**CMTMR**
Cardiac stem cells	**CSCs**
Cardiovascular diseases	**CVDs**
4',6-diamidino-2-phenylindole	**DAPI**
Endothelial basal medium	**EBM**
Electrocardiographic detection	**ECG**
Extracellular matrix	**ECM**
Endothelial nitric oxide synthase	**eNOS**
Electron transport chain	**ETC**
Fractional area change	**FAC**
Fetal bovine serum	**FBS**
Field-of-view	**FOV**

Gentamicin sulfate amphotericin-B	**GA-100**
Glyoxalase 1	**Glo1**
Glo1 over-expressing mice	**Glo1 mice**
Glyoxalase 2	**Glo2**
SH-glutathione	**GSH**
Human embryonic stem cells	**hESCs**
Heart failure	**HF**
Human Glo1	***h*Glo1**
Hypoxia-inducible factor 1 alpha	**HIF-1α**
Hematopoietic stem cells	**HSCs**
Human Umbilical Vein Endothelial Cells	**HUVECs**
Induced pluripotent stem cells	***i*PSCs**
Left anterior descending coronary artery	**LAD**
Low Serum Growth Supplement	**LSGS**
Left ventricle ejection fraction	**LVEF**
Pro-inflammatory macrophages	**M1**
Anti-inflammatory macrophages	**M2**
Methylglyoxal	**MG**
Methylglyoxal derived Advanced glycation end-products	**MG-AGEs**
Myocardial infarction	**MI**
Nitric oxide synthase	**NOS**
Phosphate Buffered Saline	**PBS**
Polymerase chain reaction	**PCR**

Platelet endothelial cell adhesion molecule	**PECAM-1**
Preproendothelin-1 promoter	**PEP8**
Quantitative polymerase chain reaction	**qPCR**
Recombinant analog of insulin-like growth factor-I	**R3-IGF-1**
Advanced glycation end-products receptors	**RAGEs**
Recombinant human epidermal growth factor	**rhEGF**
Recombinant human fibroblast growth factor basic	**rhFGF-B**
Real-time microvisualization	**RMV**
Reactive oxygen species	**ROS**
Room temperature	**RT**
Quantitative reverse transcription polymerase chain reaction	**RT-qPCR**
Standard error of measurement	**SEM**
Superoxide dismutase	**SOD**
Endothelial growth factor vascular	**VEGF**
Wild type	**WT**
Xanthine oxidase	**XO**
Alpha-smooth muscle cell actin	**α-SMA**

1. Introduction

1.1 Cardiovascular disease

Cardiovascular disease (CVD) is the leading cause of death worldwide, with more than 17.3 million deaths per year (Benjamin et al., 2017). In Canada, cardiovascular diseases is the second leading cause of death surpassed only by cancer (Public Health Agency of Canada, 2017). The risk of presenting with heart disease is double in men compared to women, in all age groups. In addition, the prevalence of CVDs is increasing as a result of aging of the Canadian population (Public Health Agency of Canada, 2017).

CVD is a group of disorders that affect the heart and the blood vessels. Among the risk factors associated with CVD are the following: family history, cigarette smoking, alcohol consumption, low physical activity, dyslipidemia, hypertension, unhealthy diet, obesity and type 2 diabetes mellitus (Public Health Agency of Canada, 2017; Weintraub et al., 2011). Myocardial infarction (MI), also known as heart attack, represents the most common form of heart disease (Public Health Agency of Canada, 2017).

1.1.1 Myocardial infarction

MI is an acute ischemic event caused mainly by a rupture of a vulnerable atherosclerotic plaque and release of its thrombogenic contents into a coronary artery. This process results in a hypercoagulable state leading to activation of platelets, initiation of the coagulation cascade and distal thrombus and embolization. The coronary artery is then partially or completely occluded, which blocks the blood perfusion with concomitant reduction of nutrients and oxygen supply to the affected area, causing regional ischemia (Reed et al., 2017; Thygesen et al., 2012). Prolonged ischemia of 2-4 hrs (Thygesen et al., 2012) can subsequently lead to necrosis of more than a

billion cardiomyocytes (Arnous et al., 2012). Since the adult mammalian heart has little regenerative capacity, this loss of cardiomyocytes has to be compensated by a cascade of cellular events that result in complex structural, functional and geometric alterations of the surviving myocardial tissue (Frangogiannis, 2014). This process of atypical remodelling comprises thinning of the ventricular wall (Burke et al., 2007), increased sphericity of the ventricle, hypertrophy of the myocardium and collagen-based scar formation (fibrosis), which altogether lead to cardiac dysfunction. Above that, adverse cardiac remodelling and progressive deterioration of the hypertrophic tissue are often associated with heart failure (HF) and poor prognosis of MI-surviving patients (Frangogiannis, 2014).

1.1.1.1 Repair and healing stages post-MI

Both the size of the infarction and the quality of cardiac repair significantly affect the MI healing time (Frangogiannis, 2014). Healing of infarct border takes on average 5-6 weeks (Thygesen et al., 2012). In humans, for small MIs, 4-6 weeks are usually enough for the healing, but from 2-3 months up to a year may be necessary in severe cases. The central area of the infarct, however, remains unhealed (Burke et al., 2007). The healing process of the infarcted heart can be divided into three overlapping stages: the inflammatory phase, the proliferative phase and the maturation phase (Frangogiannis, 2014) (Figures 1.1, 1.2 and 1.3).

1.1.1.2 First stage: inflammatory phase

The necrosis of cardiomyocytes induced by the lack of oxygen supply, activates an innate immune response, which initiates an intense and transient inflammatory reaction during the inflammatory phase of MI healing (Frangogiannis, 2014; Matsui, Morimoto, & Uede, 2010)

(Figure 1.1). In humans, this phase occurs 0-4 days after myocardial injury (Hodgkinson et al., 2016) while in mice, this whole phase takes place between 1 to 72 hours (Dobaczewski, Gonzalez-Quesada, & Frangogiannis, 2010; Nah & Rhee, 2009).

The hypoxic state during ischemia impairs vascular endothelial cell integrity, thus affecting its barrier function and increasing its permeability. This allows the infiltration of leukocytes, such as monocytes into the infarcted area (Frangogiannis, 2014; Prabhu et al., 2016). Monocytes originate from common myeloid progenitor cells in the bone marrow (Geissmann et al., 2010) and upon maturation, they circulate in the blood equipped with chemokine receptors which can respond to inflammation signals, allowing their recruitment into areas of tissue damage (Dewald et al., 2005). In response to a combination of stimuli, monocytes differentiate into pro-inflammatory (M1) macrophages (Nahrendorf et al., 2010) and together with neutrophils, they accumulate in the border zone of the infarct area (Burke et al., 2007).

After 24-48 hours, the phagocytosis of necrotic cells is established by M1 macrophages (Burke & Virmani, 2007; Matsui et al., 2010). They also release cytokines and growth factors that stimulate the proliferation of fibroblasts, monocytes, and endothelial cells (Matsui et al., 2010). These inflammatory cells are also engaged in secretion of various proteolytic enzymes and reactive oxygen species (ROS) (X. Li et al., 2016).

Altogether, this process clears the infarcted area of dead cells and extracellular matrix (ECM) debris and prepares it for the proliferative phase of healing (Frangogiannis, 2014).

1.1.1.2.1 Start of inflammation and ROS production

In response to hypoxia, both the infarcted myocardium and endothelium generate endogenous signals which activate the inflammatory cell recruitment and promote leukocyte infiltration into

the healing infarct (Frangogiannis, 2014). One of the ischemia-mediated signals is the increase in ROS (Frangogiannis, 2014).

ROS are derivatives of univalent reduction of molecular oxygen (O_2), and comprise radical superoxide ($\bullet O_2$), hydrogen peroxide (H_2O_2) and hydroxyl radical (•OH) (Bolli, 1988). In the heart, ROS can be produced by different mechanisms, including: xanthine oxidase (XO), cytochrome P450, NAD(P)H oxidases, catecholamines auto-oxidation and NO synthase (NOS) uncoupling (Giordano, 2005).

It has been shown that during acute inflammation after MI, ROS are secreted by neutrophils and monocytes (X. Li et al., 2016). ROS can be also produced during oxidative phosphorylation through electron leakage from the mitochondria (Sun, 2009). Superoxide is formed during ischemia from residual O_2 in the tissue prior to reperfusion (Vanden Hoek et al., 1997), while high amounts of H_2O_2 and •OH can be generated after an abrupt reoxygenation after reperfusion (Vanden Hoek et al., 1997).

When ROS levels surpass the antioxidant defense capacity, these free radicals react directly with proteins, lipids and DNA; damaging the cells and causing cell death (Giordano, 2005). The reperfusion onset time seems to be decisive whether positive or negative effects prevail. If reperfusion occurs within 2 to 3 hours after the ischemia onset, more benefits are observed, such as myocardial salvage and infarct size reduction. However, if reperfusion occurs later or ischemia is more prolonged, cytotoxic levels of ROS are generated (Burke et al., 2007).

This results in oxidative stress, which can further extend the ischaemic injury, irreversibly damage myocytes, cause microvessel dysfunction (Burke et al., 2007) and contribute to cardiac dysfunction (Bolli, 1988).

1.1.1.2.2 Effects on antioxidant SOD

Enzymatic and non-enzymatic mechanisms are used by the cells to counterbalance the formation of ROS. Superoxide dismutase (SOD), together with catalase and glutathione peroxidase, are responsible for scavenging oxygen metabolites (Giordano, 2005).

SOD is responsible for transforming $\bullet O_2^-$ into O_2 and H_2O_2, thus assisting in the recovery of myocardium after MI, with the possibility of increasing the contractility of myocardium. However, post-ischemic conditions cause a dysfunction of this enzyme in the mitochondria, an important site of generation of superoxide radicals (Bolli, 1988; Ferrari et al., 1985). In addition to the previously described increment of ROS production, such reduction of antioxidant reserve can lead to an effect known as oxidative stress associated with cell toxicity and cell death (Giordano, 2005; Sun, 2009).

1.1.1.2.3 Implications on cardiomyocyte viability

As previously mentioned, one of the main consequences of ischemia and reperfusion is cell death. The harmful effects of ischemia begin as early as 20-40 minutes after total occlusion of blood flow (Burke et al., 2007). Various mechanisms of cell death are activated, mainly cell necrosis, secondarily apoptosis and thirdly autophagy (Prabhu et al., 2016). The consequences can be so severe that 25% out of the 2-4 billion cardiomyocytes present in the human left ventricle can be wiped out in a few hours (Laflamme et al., 2011), especially in the central portion of the infarction (Burke & Virmani, 2007). As described above, the clearance of dead cells and ECM debris at the infarcted area marks the beginning of the proliferative phase of MI healing (Frangogiannis, 2014).

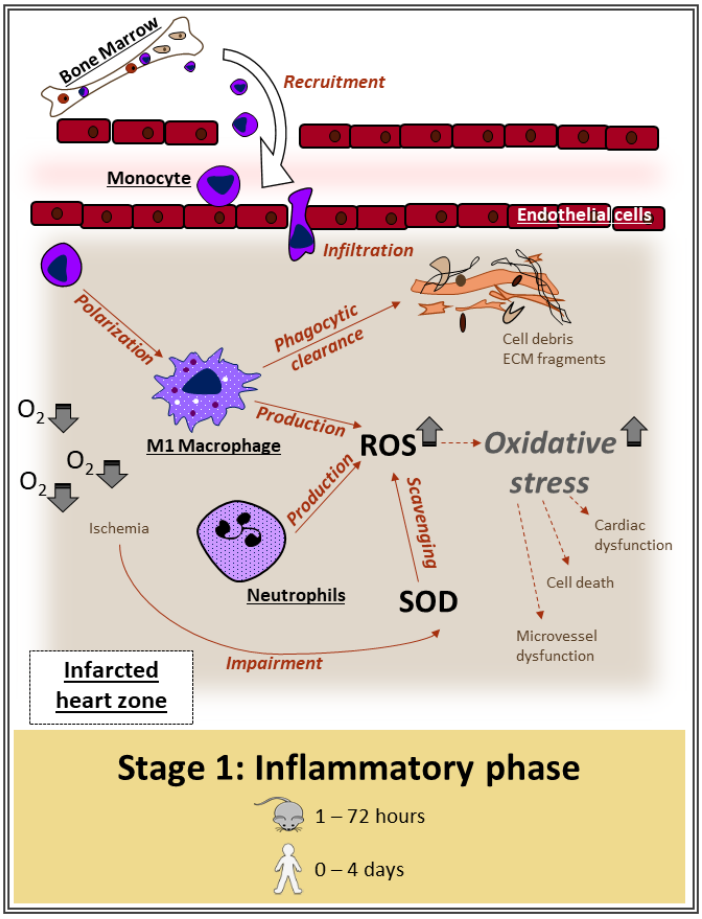

Figure 1.1. First stage of myocardial infarction healing: *inflammatory phase*. Following myocardial injury, the inflammatory response begins with the recruitment of monocytes from the bone marrow. After polarization of monocytes towards the pro-inflammatory M1 macrophages, they clear the infarcted area of cell debris and extracellular matrix fragments. In response to hypoxia, M1 macrophages together with neutrophils release reactive oxygen species (ROS) which, coupled with a decrease in the production of ROS-scavenging enzyme superoxide dismutase (SOD), cause cellular toxicity.

1.1.1.3 Second stage: proliferative phase

The early phagocytosis of apoptotic cells activates the transition from inflammatory to proliferative/repair stage by inducing inhibitory molecules, activating suppressive pathways (Frangogiannis, 2014) and initiating the conversion of pro-inflammatory macrophages (M1) to

an anti-inflammatory (M2) population (Yan et al., 2013). The proliferative phase of MI healing thus begins (Figure 1.2).

In mice, this second stage of reparation starts as early as 48 hrs and continues for up to 7 days after reperfusion (Dobaczewski et al., 2010; Nah & Rhee, 2009), while in humans it takes place at 0-3 weeks after myocardial injury (Hodgkinson et al., 2016).

In the proliferative phase, mononuclear cells and subpopulations of macrophages secrete growth factors and cytokines (Chen et al., 2013; Frangogiannis, 2014). These molecules then recruit and activate reparative mesenchymal cells, mainly fibroblasts, fibroblast-derived myofibroblasts and vascular cells, leading to the formation of granulation tissue (Frangogiannis, 2014).

This highly cellular and growth factor-rich environment allows activated myofibroblasts to synthetize collagen, matricellular proteins and contractile proteins such as alpha-smooth muscle cell actin (α-SMA) (Chen et al., 2013). And due to the enormous demands of this highly cellular and metabolically active granulation tissue on oxygen and nutrients, new vessels are necessary (Zymek et al., 2006).

1.1.1.3.1 Angiogenesis

Angiogenesis, or formation of new blood vessels by vascular cells, constitutes another step in the infarct healing (Burke et al., 2007), as it supplies the metabolically active granulation area with oxygen and nutrients (Zymek et al., 2006). In the border region of the infarction, the granulation tissue is abundant with newly generated blood vessels (Matsui et al., 2010). Later, new vessels will start to emerge as well more centrally (all dependent on the size of the infarcted area), while the previously formed vessels will have matured. This consequently leads to stabilization of the newly formed microvasculature system and to suppression of the

inflammatory reaction mainly by preventing further recruitment of leukocytes to the area (Frangogiannis, 2014).

1.1.1.3.2 Suppression of inflammation

The suppression and spatial confinement of inflammation is crucial for the proper repair of injured tissues. When the inflammation is prolonged or highly expanded, both the cardiomyocyte loss and matrix degradation are accentuated (Frangogiannis, 2014). This can further affect the integrity of the ventricular wall, causing additional dilation and possibly cardiac rupture and expansion of the fibrotic scar. All these degenerative effects together reduce or suppress the heart's systolic function (Frangogiannis, 2014). Consequently, precise spatial confinement of the inflammation is necessary for enabling the transition to the third stage of infarct healing – the maturation phase (Frangogiannis, 2014).

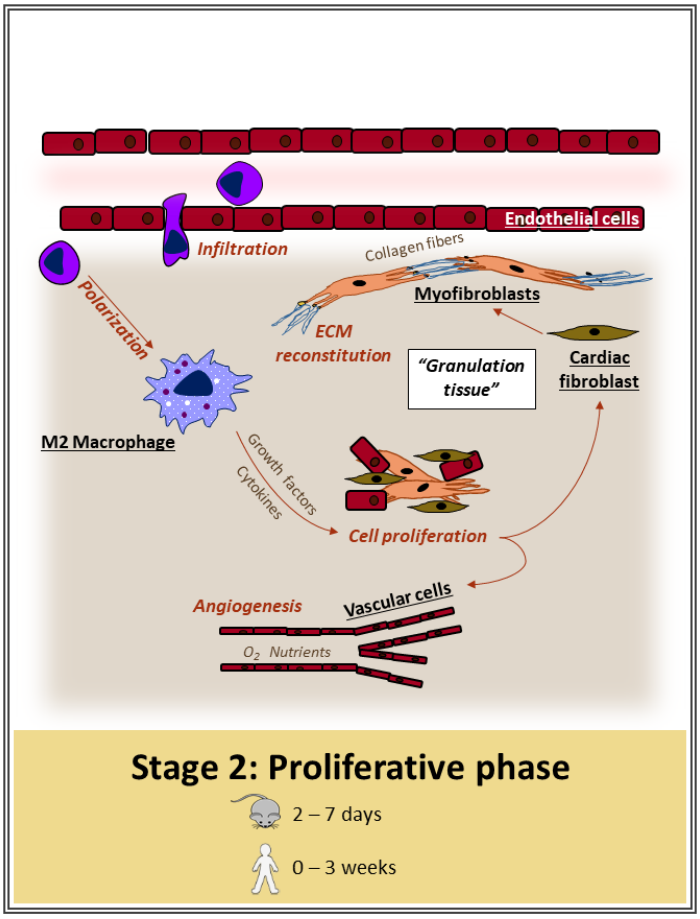

Figure 1.2. Second stage of myocardial infarction healing: *proliferative phase*. Once the infarcted area is cleared of cell debris and cell matrix fragments, the monocytes change their polarization towards the reparative M2 macrophages which release proliferation-activating chemical signals. As a result, fibroblast-derived myofibroblasts synthesize high amounts of collagen and extracellular matrix (ECM) proteins which will constitute the scar. In response to a need for greater supply of oxygen and nutrients, new vessels are formed (angiogenesis).

1.1.1.4 Third stage: maturation phase

As the scar matures and the inflammation resolves, myofibroblasts proliferate and produce abundant collagen that later replaces the highly vascularized granulation tissue with a collagen-rich scar that preserves the structural integrity of the chamber (Burke et al., 2007). The last stage of MI healing – the maturation phase – thus initiates (Figure 1.3). By the end of this stage,

the repairing cells have died by apoptosis, a scar of cross-linked collagen has been formed and the infarct has overall matured (Frangogiannis, 2014). Two areas can now be distinguished: the central zone, where the greatest loss of myocytes occurred, without any or with only very little blood flow; and the surrounding marginal zone, with new collateral vessels (Burke et al., 2007). In mouse, the formation of mature collagen scar occurs between days 5 and 28 post-reperfusion (Dobaczewski et al., 2010; Nah & Rhee, 2009). In humans, scar maturation is a process that requires more time, taking from 2 to 6 weeks to complete (Hodgkinson et al., 2016).

1.1.1.4.1 Complications of fibrosis and remodelling

Although scar formation is necessary to preserve the cardiac geometry, excessive scar deposition is associated with a decreased density of microvasculature and altered myocardial structure. This results in increased heart stiffness and left ventricle remodelling (Zeisberg et al., 2007). Such reduction in cardiac tissue elasticity can further lead to diastolic dysfunction, an important cause of heart failure (Zeisberg et al., 2007).

At the same time, the thinning of the ventricular wall caused by the loss of cellular tissue promotes a series of atypical structural changes also known as “cardiac remodelling”. Such progressive cardiac complication includes ventricular shape shift from elliptical to spherical or myocardial hypertrophy. Furthermore, when coupled with fibrosis and gradual deterioration of the hypertrophic tissue (incapable of regenerating cells), it can lead to heart failure and death (Arnous et al., 2012; Orlic et al., 2001).

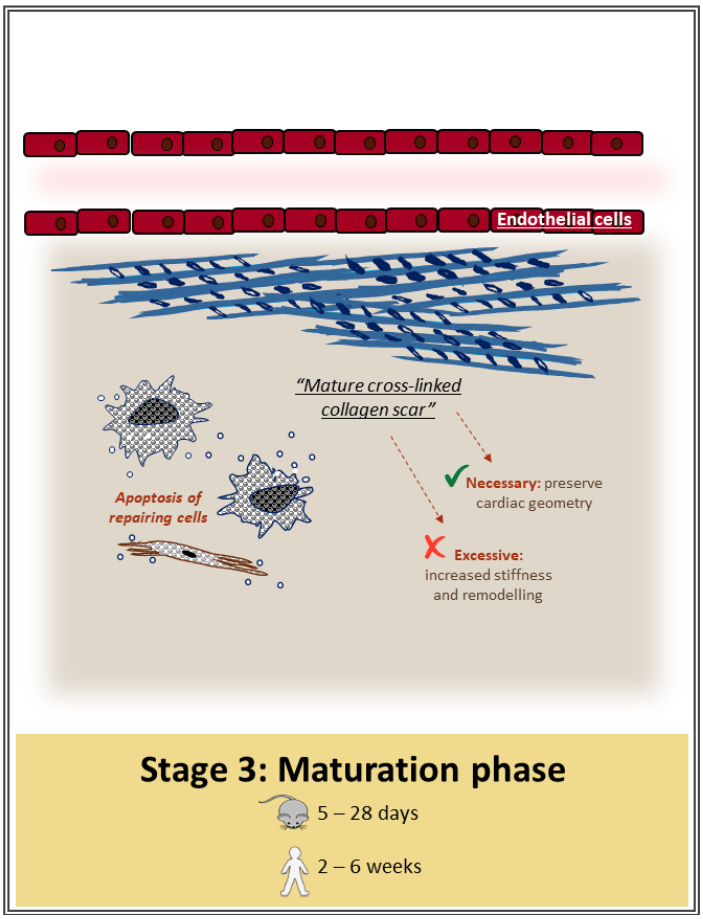

Figure 1.3. Third stage of myocardial infarction healing: *maturation phase*. The myofibroblast-produced collagen fibers cross-link and the scar matures. The inflammation is reduced, and the repairing cells die by apoptosis.

1.2 Current therapies

Several therapeutic approaches have been developed and used to treat MI. In the early 1970s, new pharmacological agents, such as β-adrenergic-receptor blockers, were successful in treating MI. In 1980, mortality was decreased with the emergence of therapies that dissolved blood clots and restored blood flow. Nowadays, treatments that aim to improve quality and duration of life include both non-invasive and invasive approaches. Non-invasive strategies include the use of: (i) antiplatelet agents, (ii) anticoagulant agents, (iii) angiotensin-converting enzyme (ACE)

inhibitors, (iv) angiotensin II receptor blockers, (v) statins, and (vi) thrombolytic agents (fibrinolysis). Invasive approaches comprise: (i) open-heart surgery, (ii) catheter-based interventions that open clogged arteries, (iii) use of (hybrid) metallic stents to reopen the blood vessels and prevent the restenosis, and (iv) coronary artery bypass grafting, among others (Braunwald, 1997; Kwon et al., 2010; Reed et al., 2017).

Nonetheless, despite the optimization in these cardiovascular medications or mechanical interventions after MI, the mortality from medium to long term remains as high as 7-12% (Mathur et al., 2017). Partially, this is because these therapies are not aimed at replacing lost cardiac cells or restoring blood vessels, but rather to preserve or maintain cardiac function (Arnous et al., 2012). Since the cardiomyocytes within mammalian heart have little capacity for recovery, heart transplantation is left as the only current strategy addressing severe loss of cardiomyocytes and heart dysfunction. Its use, however, is hampered by the rigorous selection criteria and low number of potential donors (Laflamme et al., 2011). Therefore, the development and improvement of therapies that delay the heart's deterioration and/or repair the damage that occurs after a cardiovascular event is crucial. For this reason, a new interdisciplinary field - regenerative medicine – has emerged in the last decades, with the ultimate goal of regenerating the damaged myocardium.

This interdisciplinary field uses tools and advances in the areas of cell therapy, developmental biology, and biomaterials, among others (Laflamme et al., 2011). Regenerative medicine and cell therapy offer a potential treatment option for the infarcted heart by restoring or preventing the loss of cardiomyocytes and enhancing neovascularization; which are two features necessary to reverse the effects of cardiac remodelling (Lemcke et al. , 2018).

1.3 Regenerative medicine

Regenerative medicine is dedicated to the search of therapeutic strategies that restore or regenerate cells, tissues or organs, to improve the quality of life. During the last decades, various cell therapies have been proposed to restore/regenerate the infarcted hearts using hematopoietic stem cells (HSCs), cardiac stem cells (CSCs), bone marrow cells (BMCs), adipose-derived stem cells, skeletal myoblasts, and embryonic stem cell-derived cardiomyocytes, among others (Laflamme et al., 2011; Murry et al., 2006).

Trials with stem/progenitor cell transplantation have shown promising results, such as: reduction of infarct size, restoration of myocardial perfusion and enhancement in left ventricular systolic function. These results, however, differ between studies and are difficult to compare due to diverse methods used for cell isolation, processing and identification, and varying dosage and timing of introduction (Kwon et al., 2010).

Human embryonic stem cells (hESCs) have the highest differentiation capacity and may be more useful for treating MI; however, their use is hindered by technical and ethical issues that would need to be addressed first. On the other hand, induced pluripotent stem cells (iPSCs) have shown differentiation capacity into cardiac cells, restoring cardiac, smooth muscle and endothelial tissues (Kwon et al., 2010). IPSCs are a promising option for cell therapy, however this area requires more work due to the plasticity potential of these cells which could lead to teratoma formation (Kandaswamy et al., 2018).

Despite their limited differentiation capacity, adult stem cells are the best currently available option for cardiac cell therapy since they have the advantage of being autologous, thus minimizing immune rejection. One promising source of adult stem cells are the BMCs, which originate in the bone marrow (Arnous et al., 2012).

1.3.1 Cardiac therapy with bone marrow cells

BMCs are arguably the most widely used clinically relevant cells for treating MI. The mononuclear fraction of BMCs consists of a heterogeneous population including mesenchymal stem cells, haematopoietic progenitor cells and endothelial progenitor cells (Arnous et al., 2012). They have the potential of self-renewal, proliferation and multi-directional differentiation towards hematopoietic and non-hematopoietic fate. They have been also shown to promote the restoration of damaged tissue, to have low immunogenicity; and to be easily obtained, cultivated and amplified, thus making them a viable candidate for cell therapy (Kwon et al., 2010; J.-R. Li al., 2017). On top of that, they are considered as one of the safest for cell therapy purposes due to their limited plasticity, thus making tumor formation or the onset of arrhythmias less likely (Murry et al., 2006).

Therapy with BMCs has been demonstrated to promote neoangiogenesis, increase myocardial viability and reduce fibrosis and inflammation in post-infarcted hearts. Paracrine effect of BMCs rather than their direct differentiation/cell replacement is considered as their principal mechanism of function. When the BMCs are transplanted into the hypoxic post-infarct environment, they release a variety of cytokines, chemokines and growth factors. These paracrine signals in turn influence the adjacent host cells, and thus promote vasculogenesis and angiogenesis (Arnous et al., 2012; Orlic et al., 2001).

1.3.1.1 Modest outcome of therapies with BMCs

Although the potential of BMC-based therapies has been demonstrated in both animal models and clinical trials (see Arnous et al., 2012 for a review), the associated benefits remain modest at best. Although the precise underlying mechanisms are not fully understood yet, low cell viability

and poor retention in the treated area are considered the two main challenges with regard to this therapeutic approach (Arnous et al., 2012; L. Li et al., 2013). Low survival of transplanted BMCs in the post-ischemic heart environment might be caused by a combination of the following factors: immune responses, inflammatory mechanisms, low oxygen (X. Li et al., 2016), and locally increased ROS formation; which in turn induce cell apoptosis (L. Li et al., 2013).

1.3.1.2 Possible approaches for the improvement of BMC therapy

Several approaches have been proposed to overcome the low cell survival and retention. The following have been mainly investigated: (i) biomaterials, in order to improve cell retention at the site, (ii) pre-acclimatization and protection of cells from the hostile post-infarct conditions (X. Li et al., 2016), and (iii) overexpression of cytoprotective genes (Lemcke et al., 2018; L. Li et al., 2013; Singh et al., 2016). Hence, opportunities for further enhancement in stem cell therapy still lie ahead.

1.4 Methylglyoxal

One of the molecules that contribute to the hostility of the post-MI environment and that could be targeted in order to improve the survival of transplanted cells is 2-oxopropanal, more commonly known as methylglyoxal (MG) (Blackburn et al., 2017). MG is a highly reactive dicarbonyl, 200 - 50,000-fold more reactive than glucose (Rabbani et al., 2008). It is produced during: (i) the metabolism of ketone bodies, (ii) lipid peroxidation, (iii) degradation of threonine, (iv) fragmentation of glycated proteins, and mainly, (v) by degradation of triose phosphates (Thornalley, 2003; Thornalley et al., 1994; Thornalley, 2004) (Figure 1.4).

MG can cross cell membranes by passive diffusion (Abordo et al., 1999), thus interacting with nucleic acids, proteins and lipids both intra- and extra-cellularly (Thornalley, 2008). MG reacts non-enzymatically with lysine and arginine residues of proteins and forms irreversible advanced glycation end-products (AGEs, Figure 1.4). These modifications can alter the structure and function of proteins, leading to cellular and tissue dysfunction, also known as "dicarbonyl stress" (Thornalley, 2003).

Furthermore, AGEs can interact with AGE receptors (RAGEs) found in monocytes, macrophages, endothelial cells, and pericytes, among others (Thornalley, 1998) and this can lead to inflammatory responses, programmed cell death, oxidative stress (Thornalley, 1998) and vascular cell dysfunction (Thornalley, 2004). Additionally, MG can modify DNA, forming nucleotide AGEs, which are associated with increased mutagenesis and cell death; while excessive lipid glycation is related to membrane lipid bilayer disruption (Thornalley, 2008) (Figure 1.4).

1.4.1 Glyoxalase system

Under healthy physiological conditions, the glyoxalase system composed of glyoxalase 1 (Glo1) and glyoxalase 2 (Glo2), along with the cofactor SH-glutathione (GSH), provides protection against MG and its associated AGEs. The glyoxalase system, present in the cytosol of cells, catalyzes the transformation of reactive acyclic α-oxoaldehydes, such as MG, into their corresponding non-toxic α-hydroxyacids (Thornalley, 2003).

The primary enzyme that metabolizes and prevents the accumulation of MG is Glo1 through a GSH-dependant mechanism (Shinohara et al., 1998). In this reaction, Glo1 catalyses the isomerization of the hemithioacetal (CH_3COCH(OH-SG)), spontaneously formed from

methylglyoxal (CH_3COCHO) and GSH, into S-D-lactoylglutathione [$CH_3CH(OH)CO$-SG] (Thornalley et al., 1994). Glo2 then catalyzes the hydrolysis of S-D-lactoylglutathione into D-lactate ($CH_3CH(OH)CO_2$), while also replenishing GSH for the next metabolic reaction (Shinohara et al., 1998) (Figure 1.4). Finally, D-lactate is excreted in urine or absorbed by gut bacteria (Rabbani et al., 2016).

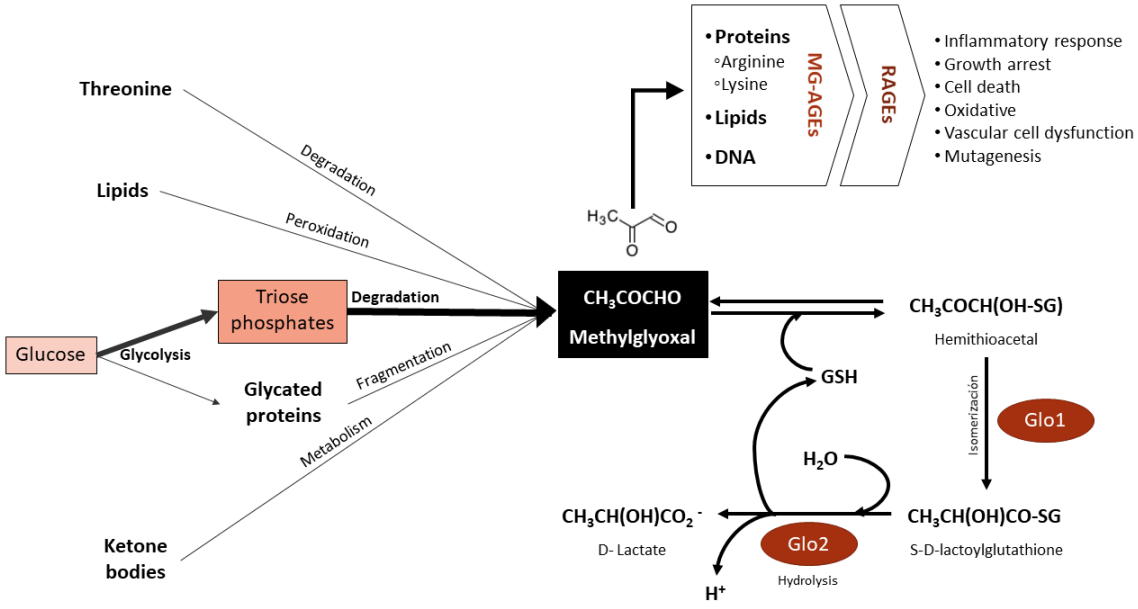

Figure 1.4. Methylglyoxal. Methylglyoxal (MG) is formed through diverse metabolic pathways, but mainly by degradation of triose phosphates. The Glyoxalase system, composed by Glyoxalase 1 and 2 (Glo1 and Glo2, respectively), transforms MG into non-toxic D-Lactate, thus preventing the development of MG-advanced glycation end-products (MG-AGEs) which can affect cell function and viability through their interaction with receptors of AGEs (RAGEs).

1.4.2 Increased accumulation of MG post-MI

Glo1 is considered the main enzyme responsible for detoxification of MG and thus the most important for the cellular anti-glycation defense. Nevertheless, under conditions of hypoxia, ischemia and inflammation (all present post-MI), the production of MG is increased with a

simultaneous drop in Glo1 activity (Rabbani et al., 2016). Different mechanisms are involved in this outcome.

For one, oxidative stress is related to the accumulation of MG-modified proteins (Thornalley, 2008), particularly in the mitochondria (Rosca et al., 2005). Proteins within complexes III and IV of the mitochondrial electron transport chain (ETC) are major targets for dicarbonyl glycation. These complexes are in turn the main site of ROS production since superoxide is continuously generated as a by-product of the electron transport (Rosca et al., 2005). Superoxide production is increased during ischaemic damage because glycation of the aforementioned ETC complexes causes mitochondrial dysfunction and results in electrons not being transferred between elements of the ETC, but being donated to molecular oxygen instead (Lesnefsky & Hoppel, 2003). Successively, this oxidative stress depletes GSH; and since Glo1 activity is proportional to GSH concentration, Glo1 efficiency decreases (Thornalley, 2003) leading to further MG accumulation. Thus, ROS and MG propagate each other in a loop.

Moreover, under ischemic conditions cells cannot rely on oxidative phosphorylation for the generation of adenosine triphosphate (ATP), because this pathway depends on the availability of oxygen. Therefore, cardiac cells are forced to undergo a metabolic shift from aerobic metabolism to anaerobic glycolysis to generate energy (Kalra et al., 2012). This change favors the formation of MG and the accumulation of fatty acids and lactate (Rabbani et al., 2016).

Taken together, all these factors result in MG accumulation to cytotoxic levels, which result in increased oxidative stress, protein glycation, tissue damage and hostility of the cellular environment in the ischaemic area (Thornalley, 2003).

1.4.3 Role of MG in cardiomyopathies

MG effects have been widely studied in diabetic cardiomyopathies (Hanssen et al., 2017, 2018; Schalkwijk, 2015; Vulesevic et al., 2016), but little attention has been given to non-diabetic heart complications. Out of the few publications that deal with non-diabetic conditions, the following deserve interest. For example, an association between infarction and concomitant ischemia with an increase in MG and AGE production in the heart after reperfusion has been demonstrated (Aleshin et al., 2008; Bucciarelli et al., 2006). Moreover, an increase in MG-derived AGEs (MG-AGEs) has been reported in human carotid rupture-prone atherosclerotic plaques, with associated augmentation of inflammatory mediators and apoptosis (Hanssen et al., 2014). In a previous publication from our laboratory (Blackburn et al., 2017), MG-AGEs were associated with the impairment of cardiac function post-MI. Accumulation of MG-AGEs in infarcted heart was demonstrated at 6 hours post-MI with persistence for up to 4 weeks, suggesting that MG might affect both short-term and long-term wound healing, in addition to contributing to adverse remodelling and cardiac dysfunction.

1.4.4 Overexpressing Glo1 has prevented MG toxic effects

The protective effects of Glo1 overexpression have been demonstrated in diabetes studies *in vitro* by reducing the levels of MG (Shinohara et al., 1998) as well as by protecting against dicarbonyl glycation and correcting defective hyperglycemia-induced angiogenesis (Ahmed et al., 2008). *In vivo*, Glo1 overexpression reduced the level of carbonyl stress, AGEs and oxidative stress (Brouwers et al., 2011), inhibited retinal AGE formation and prevented lesions of diabetic retinopathy (Berner et al., 2012), and partially corrected the impaired formation of arteries in the ischaemic hindlimb (Brouwers et al., 2016). A previous study from our lab (Vulesevic et al.,

2016) demonstrated in a murine model of diabetes the protective effect of Glo1 overexpression by displaying reduced vascular inflammation and lower carbonyl stress in the myocardium, delayed and limited loss of cardiac function, preserved endothelial cell number in the myocardium and preserved capillary density. In the same study, endothelial cells were transfected with a Glo1-overexpressing plasmid and these cells were more resistant to death upon exposure to MG. Additionally, another study from our lab (Vulesevic et al., 2014) demonstrated that a Glo1 overexpressing bone marrow transplant can preserve the circulating angiogenic cells' viability, mobilization and recruitment and overcome defective neovascularization in ischaemic hindlimbs of an *in vivo* model of diabetes.

In a non-diabetic MI model, our lab (Blackburn et al., 2017) demonstrated that the prevention of MG accumulation by overexpressing Glo1 in the vasculature and bone marrow led to reduced cardiomyocyte apoptosis and infarct size. Furthermore, Glo1-overexpressing mice were conferred with superior cardiac function, preserved ventricular geometry, increased vascular density, and enhanced c-kit^{+} cell recruitment and incorporation into vasculature when compared to wild type (WT). In summary, these results identify MG as a potential target to improve the effectiveness and outcome of cellular therapies.

As previously stated, although different cell types have shown promising results in heart regeneration, cell therapy is currently far from efficient (X. Li et al., 2016). The present study therefore aimed at improving the outcome of BMC therapy by targeting the negative effects of MG using Glo1- overexpressing BMCs.

2. Hypothesis

It was hypothesized that overexpressing Glo1 in BMCs would improve their viability and retention when transplanted into the MI heart, and thus translate into a better cell therapy response.

3. Experimental aims

AIM 1. To evaluate the ability of Glo1-overexpression to improve the function of BMCs after exposure to MG *in vitro*. Functional analyses included: viability, ROS and SOD production, angiogenic potential, and migration.

AIM 2. To evaluate the ability of Glo1-overexpressing BMCs to confer superior therapeutic effect in a mouse model of MI in terms of preserved cardiac function, reduced formation of scar and increased vascularity in the infarct and peri-infarct areas.

4. Materials and methods

For a schematic summary of the present study, refer to figure 4.1.

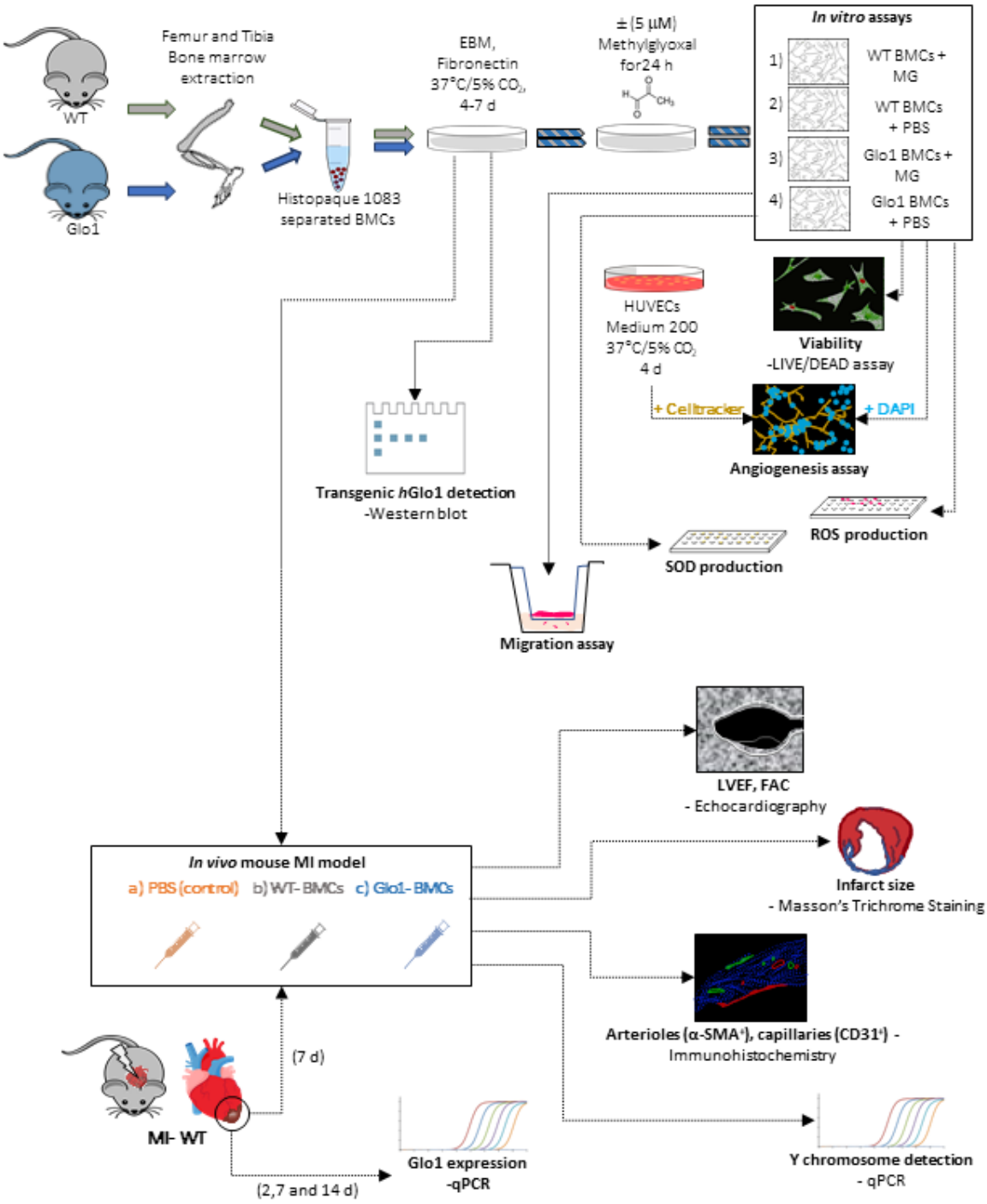

Figure 4.1. Schematic summary of the present study.

4.1 Aim 1 *in vitro* studies

Transgenic *h*Glo1 mice

All experimental procedures were performed with the approval of the University of Ottawa Animal Care Committee and in accordance with the National Institute of Health Guide for the Care and Use of Laboratory Animals. Human Glo1 over-expressing mice (Glo1 mice) were bred on a C57/BLJ6 background and carried a transgene encoding human Glo1 (*h*Glo1) with a c-myc epitope tag under the control of the preproendothelin-1 promoter (PEP8), as previously reported (Vulesevic et al., 2014). The genotyping of mice or 7d-cultured BMCs was performed by end-point PCR using the following primers specific for the *h*Glo1 transgene construct: 539 F: 5'-CTG ACG CGT TGC TAG CAG AAC CGC AGC CCC-3', and 1125 R: 5'-TCT CAG CTC TAG AGA TAT CAC TAC ATT AAG-3'; and visualized on a 1% agarose gel.

All experiments used mice hemizygous for the *h*Glo1 transgene or their non-transgenic littermates. Glo1 mice were previously characterized by the lab, showing that despite the expected endothelial-specificity of the promoter, bone marrow derived-macrophages showed five-fold higher Glo1 activity compared to WT littermates (Vulesevic et al., 2014).

Bone marrow extraction for *in vitro* studies or *in vivo* injections

Unless otherwise indicated, both male and female, WT and Glo1 C57/BLJ6 mice (7-10wk old) were used as a BMC source. Mice were euthanized by CO_2 inhalation followed by cervical dislocation. Both ends of the femoral and tibial epiphyses were cut off and bone marrow was flushed out using a 27-gauge needle and phosphate buffered saline (PBS). The isolated bone marrow was centrifuged at 250*g* for 10min. The pellet was resuspended in PBS and added to Histopaque 1083 (Sigma) at a ratio 1:1. The mixture was centrifuged at 400*g* for 30min to

separate the cells by density gradient. The middle layer, which was white and cloudy containing a heterogeneous cell population (including mononuclear cells), was gently removed and transferred to a new centrifuge tube. The cells were twice centrifuged at 300*g* for 10min followed by washing with PBS and then seeded onto fibronectin-coated plates in endothelial basal medium (EBM; Clonetics) supplemented with 5% FBS, rhFGF-B, R^3-IGF-1, hydrocortisone, GA-1000, rhEGF, VEGF and ascorbic acid (Lonza). For *in vitro* studies, BMCs of each mouse were divided into 2 wells, one for each treatment (see below), while for the *in vivo* study, donor BMCs were cultured in only one Petri dish. Cultures were maintained at 37°C in a humidified 5% CO_2 incubator for 4-7 days until the cells reached confluence. To remove non-adherent cells, the medium was replaced after 2-4 days and one day before treatment. The adherent cells that were generated by this procedure were previously published (Vulesevic et al., 2014) to express the following markers: 16.7 ±1.2% FLK^+, 2.0 ±0.3% $CXCR4^+$, 29.2 ±0.9% c-kit^+, and 5.8 ±1.0% $CD34^+$ cells.

MG treatment for *in vitro* studies

Following culture for 4-7 days, 5μM MG (Sigma-Aldrich) or PBS as a negative control were added to WT and Glo1 BMC cultures. Unless otherwise specified, exposure to treatment lasted 24h at 37°C/5% CO_2 after which, cells and/or conditioned media were collected. ±MG treated WT and Glo1 BMCs were evaluated for viability, angiogenesis, intracellular ROS content, and SOD production, as described below. Conditioned media collected from these cultures were used to assess their chemoattractant properties for the migration of endothelial cells.

Trypsinization procedure

Cells were lifted from the cell culture dishes or well plates using 0.25% trypsin previously warmed up to 37°C. Cells were rinsed twice with PBS, treated with trypsin, and incubated 5min/37°C. Next, 100 µl of FBS per ml of trypsin solution was added and cells were centrifuged at 250*g*/5min.

***In vitro* viability assay**

BMCs were cultured in a 24 well-plate and exposed for 24h or 48h to ±5µM MG. Then, WT and Glo1 BMC media were removed and stored at -80°C as conditioned media for future experiments. Wells were washed with PBS and cells were stained using the LIVE/DEAD® Viability Assay Kit (Invitrogen). This kit includes green-fluorescent calcein- acetoxymethyl (calcein-AM), which labels intracellular esterase activity, therefore staining live cells; and red-fluorescent ethidium homodimer, that binds to DNA of cells with damaged membrane, thus detecting dead cells. Cells were imaged using a Zeiss Z1 fluorescence microscope assisted by the AxioVision digital image software (three images/sample, ×40 magnification). ImageJ was used to adjust the contrast and enhance the distinction of colours, and to count cells in a blinded fashion. Viability was calculated per field-of-view (FOV) as: viable cells/total cells.

Intracellular Reactive Oxygen Species (ROS)

WT and Glo1 BMCs were tested for intracellular ROS production. To assess this, the Cellular ROS Detection Assay Kit (Deep Red Fluorescence; Abcam) was used. This kit contains a cell-permeable dye that generates red fluorescent signal after reacting with ROS (Ex/Em=650/675 nm). After 5 days of culture, cells were trypsinized, counted and seeded in a fibronectin-coated 96-well plate ($4x10^4$ cells per well, 6 wells per sample), and incubated for 24h to allow adhesion.

Following that, one well of each sample was exposed either to 5μM MG or PBS, in duplicate, and incubated for 24h in EBM. One set of wells (n=2) per sample was left untreated. A set of 3 wells was coated with fibronectin and EBM was added, but no cells, and was used as blank. ROS deep stain working solution was prepared following the manufacturer's protocol. As a positive control, the untreated set of wells per sample was exposed to 10μM H_2O_2 and put back into incubation for 30 min. Fluorescence was read at Ex/Em= 650/675nm with bottom read mode using a fluorometric microplate reader. All incubations were performed at 37°C/5% CO_2.

SOD production

The EnzyChrom™ Superoxide Dismutase Assay Kit (BioAssay Systems) was used to quantify the production of superoxide dismutase (SOD). This kit contains a WST-1 dye that reacts with O_2^- produced by xanthine oxidase (also provided by the kit) and forms a coloured product. In the presence of SOD, less O_2 is available for the chromogenic reaction since SOD scavenges the O_2^-. The colour intensity can be detected by spectrophotometry at OD= 440nm. After 24h exposure to ±5μM MG, BMC cultures were washed with PBS and proteins were extracted with cold lysis buffer (50mM potassium phosphate, 0.1mM EDTA, 0.5% Triton X-100), on ice. After 10 min, cell debris was collected using a rubber policeman and the extract was centrifuged at 12,000*g*/5min. Supernatant was carefully transferred to a new tube and protein concentration was quantified using the Pierce BCA protein assay (Thermo Scientific), using the standard curve as reference. Samples were diluted in PBS so that all of them would have 60μg/ml. Each sample and SOD standard provided by the kit was loaded into a different well in duplicate into a 96-well plate. Following the manufacturer's protocol, the Working Reagent and diluted xanthine oxidase from the kit was added to each well. The plate was immediately read at OD= 440nm and once more

after one-hour incubation at room temperature (RT) in the dark. SOD concentration (U/ml) of samples was calculated following the manufacturer's instructions.

***In vitro* angiogenesis**

After 24h exposure to ±5μM MG, half the media from WT and Glo1 BMCs cultures were removed and stored at -80°C as conditioned media for future experiments. Cells in the remaining media were stained with 1:100 DAPI (Sigma) and incubated for 30 min. At the same time, Human Umbilical Vein Endothelial Cells (HUVECs; passages 11-16), previously maintained in M200 media supplemented with LS-GS (Gibco) until 80% confluency, were stained with 1:500 Celltracker orange CMTMR (Invitrogen). Following a PBS rinse, cells were trypsinized as described above and counted. Then, $7x10^3$ BMCs were co-cultured with $7x10^3$ HUVECs in *in vitro* angiogenesis μ-slides (IBIDI) coated with ECMatrix™ (Millipore) in M200 media. $1x10^4$ HUVECs were seeded in other wells as control. After overnight incubation at 37°C/5% CO_2, wells were imaged using a Zeiss Z1 fluorescence microscope assisted by the AxioVision digital image software (×2.5 magnification). ImageJ was used to adjust the contrast and enhance the distinction of elements and to measure total network length in millimeters and quantify BMCs incorporated into tubular structures in a blinded fashion.

Chemotaxis migration assay

Migration was assessed using a vertical Costar Transwell two-chamber system with a 6.5mm filter diameter and a pore size of 5μm. Briefly, $2×10^4$ HUVECs were loaded into the upper chamber in M200 media with 0.3% FBS. The bottom chamber was filled with 300μl of one of the following chemo-attractants: (i) conditioned media obtained from ±MG-treated Glo1 and WT BMC cultures used for viability and angiogenesis assays, (ii) complete M200 media with 15%

FBS, or (iii) serum/growth factors-free M200 media. After incubation for 24h/37°C, cells were washed with PBS, fixed in 4% formic acid for 10 min and stained with DAPI (1:100). The number of cells that migrated towards the chemo-attractant was visualized and quantified with a Zeiss Z1 fluorescence microscope assisted by the AxioVision digital image software (3 images/sample, ×10 magnification).

4.2 Aim 2 *in vivo* studies

Experimental MI model

Female WT C57BL6/J mice (7-10wk old; Jackson Laboratories) were anesthetized using 2.5% isoflurane, intubated and kept under mechanical ventilation. The heart was exposed via fourth intercostal thoracotomy and MI was induced by permanent ligation of the left anterior descending coronary artery (LAD) with a 7-0 silk suture 2mm below the tip of the left atrium. All surgeries were performed by the same animal technician blinded to the treatment assigned. The mice were given a code number associated with the study protocol but not the treatment. The treatment administered to each mouse was recorded and only revealed once the functional, histological and molecular analyzes were completed. Echocardiographic tracings, histologic evaluations and qPCR tests were performed by me and one or more members of the research team who were blinded to treatment allocation to corroborate the accuracy of the results.

Injections of treatments and cardiac echocardiography

Using an ultrasound guided closed-chest procedure, mice randomly received one of the following 50µl treatments (in 5 equivolumetric injections using a 27G needle) into the infarct border zone: (1) ~3.5×10^5 WT BMCs; (2) ~3.5×10^5 Glo1 BMCs; or (3) PBS (Sigma) as control. The syringe was secured in a micromanipulator (VisualSonics), and both the needle and real-time

microvisualization (RMV) scanhead probe were aligned along the heart long axis before the injection procedure. Cardiac function was assessed at baseline (1-wk post-MI) and end-of-study (4-wk post-MI) by left ventricular ejection fraction (LVEF) and fractional area change (FAC) in a blinded fashion by echocardiography. Echocardiography was performed by parasternal long axis views using a Vevo770 system (VisualSonics) in B mode with the use of a 707B series RMV scanhead probe. Tracings were performed using the manufacturer's supplied software. Exclusion criteria: the average ±standard deviation of baseline % LVEF from all mice was calculated to establish the range of values that would be included in this study. All values falling outside of {28.76% - 50.74 %} were discarded since some mice showed lack of substantial infarct induction. Hence, a total of 8 mice were excluded from all *in vivo* assessments. Additionally, 1 mouse died after MI induction, before receiving treatment.

Infarct histology

Five Glo1 BMC-treated mice, five WT BMC-treated mice and 8 PBS-treated mice were sacrificed at 4 weeks (3wk post-treatment) and hearts were collected, perfused with 2-3ml of saline, snap frozen in OCT and stored at -80°C. Slides were prepared with 12µm sections at different levels. Sections with equal distance from the apex were chosen on all hearts. Masson's Trichrome staining was performed to measure the relative infarct size since it can differentially stain collagen deposition (blue) and healthy cardiac muscle (red). After staining, slides were coverslipped and photographed using a Celestron Digital Microscope Pro and the software provided by the manufacturer. ImageJ was used to adjust the contrast and enhance the distinction of colours. Relative infarct size was blindly assessed by the midline-arc method as previously described (Takagawa et al., 2007), in which infarct length includes all tissue that has suffered a thinning and a blue coloration, plus 50% of the transition area between the

collagenous scar and the healthy tissue. Subsequently, the infarct length was divided by the total myocardium length to obtain the percentage of scar formation.

Immunohistochemistry

To compare vascular growth induction between treatments, heart sections were obtained following the above described protocol. Sections were next labeled with rabbit anti-α-smooth muscle actin (αSMA, 1:250; Abcam) and rat anti-PECAM-1/CD31 (1:100, Santa Cruz Biotechnology) monoclonal antibodies. After that, 488 goat anti-rabbit IgG and 555 goat anti-rat IgG (both 1:600, Invitrogen) were used as secondary antibodies. Slides were mounted in DAPI fluorescent medium and coverslipped. Structures positively labelled for α-SMA$^+$ (vascular smooth muscle cells, representing arterioles) or CD31$^+$ (endothelial cells, constituting capillaries), combined with characteristic vessel morphology, were quantified in 3 random FOV on the infarcted area, and 2 random FOV on the peri-infarct area (border zone). Microscopy images were taken using a Zeiss Z1 fluorescence microscope assisted by the AxioVision digital image software. ImageJ was used to adjust the contrast and identify structures that were quantified in a blinded fashion.

4.3 Molecular analyses

Levels of G*lo*1 expression

Two, seven and fourteen days after LAD ligation, hearts of untreated infarcted mice were collected and perfused with 2-3ml of saline. Hearts of healthy mice were harvested as control. The left ventricular infarct site, and the corresponding area in the healthy control, was cut and immediately frozen in liquid nitrogen. Heart samples were stored at -80°C until needed.

RNA isolation

Using liquid nitrogen, heart segments were grinded and treated with 1 ml of TRI Reagent (Trizol, Thermofisher) and incubated at RT/5min. The resulting solution was transferred to a 1.5 ml Eppendorf tube, 200 µl of chloroform was added, and then mixed. The isolate was then incubated at RT/5min and centrifuged at 12,000*g*/15 min. The top phase was collected and transferred to a new tube where an equal volume of isopropanol was added and incubated at RT/5min or left overnight in the freezer at -20°C. The isolate was then centrifuged at 12,000*g*/10min and the supernatant was discarded. The pellet was washed with 1 ml of ice cold 75% ethanol and spun at 7,500*g*/5min. The pellet was dried and resuspended in sterile molecular biology reagent water.

cDNA preparation

The isolated RNA was converted to cDNA to be used in RT-qPCR analysis. cDNA was prepared with the BIORAD MyCycler machine using the following protocol: 72°C/3min, 4°C/30sec, 20°C/10min, 42°C/60min, 75°C/15min, and 4°C/30min. Two master mixtures were prepared. The first master mixture contained 1 µl of 10mM dNTP Mix, 1 µl of 20µM Random Hexamers, and 4.5 µl of RNA per reaction. This master mixture was created at the beginning of the procedure, placed in the machine, and the protocol was started. Once the protocol reached the 20°C stage, the reaction tubes were removed from the MyCycler machine and the second master mixture was added. The second master mixture contained 2 µl of 5x First-Strand Buffer, 1 µl of 20mM DTT, and 0.5 µl of 100U/µl SMARTScribe Reverse Transcriptase per reaction. The reaction tubes were then placed back into the MyCycler machine and the protocol continued until completion.

RT-qPCR

RT-qPCR analysis was performed to determine expression of *Glo*1 and 18S mRNA at 2 days (n=8), 7 days (n=9) and 14 days (n=8) post-MI induction. RT-qPCR was performed with the BIORAD iCycler Machine using the following protocol: 95°C/2min, 45 cycles of 60°C/15sec and 72°C/20sec with fluorescence readings, followed by 55°C/30sec, 95°C/30sec, and 60°C/1min. Each reaction contained 10 µl of 2x SensiFAST SYBR No-ROX Mix, 1 µl of 10x iCycler iQ External Well Factor Solution, 0.8 µl of 20µM primers (0.4 µl forward primer, 0.4µl reverse primer; see Table 4.1 for primer sequences), 1 µl of cDNA, and 7.6 µl of sterile molecular biology reagent water.

Gene	Direction	Sequence
18S	Forward	5'- AAA CGG CTA CCA CAT CCA AG -3'
	Reverse	5'- CCT CCA ATG GAT CCT CGT TA -3'
*Glo*1	Forward	5'- ACC CTC GTG GAT TTG GTC AC -3'
	Reverse	5'- GCC GTC AGG GTC TTG AAT GA -3'

Table 4.1. Primer sequences used for detection of G*lo*1 expression.

18S was used as a housekeeping gene and mRNA expression was expressed relative to the 18S control. Changes in mRNA expression were analyzed using the Δ-ΔC_t method. Briefly, the threshold cycle (C_t) value of 18S was subtracted from the C_t values of Glo1, calculating Delta C_t (ΔC_t). Next, the average ΔC_t value of the healthy group was subtracted from each of the ΔC_t values of healthy and 2d, 7d and 14d infarcted mouse samples using the following formula: $\Delta\Delta C_t = 2^{(\Delta Ct - HG\Delta Ct)}$. Lastly, the relative expression of G*lo*1 at 2d, 7d and 14d post-MI was calculated by dividing $\Delta\Delta C_t$/HG$\Delta\Delta C_t$. An outlier test performed with GraphPad Prism software (Grubb's

test) identified one outlier in the 7d- and one in the 14d-post MI groups, which were excluded from the results.

Detection of donor cells at 21 days after injection

To determine donor cell retention in the hearts at 3 weeks post-injection, male mice were used as BMCs donors and MI female mice as recipients so that the Y chromosome could be used as a detection marker. Three Glo1 BMC-treated and 3 WT BMC-treated mice were sacrificed, and their hearts were collected and perfused with 2-3 ml of saline. The heart of one donor male mouse (non-MI) was harvested as a Y chromosome control. The infarct and border zones were cut and kept together in a 1.5 ml Eppendorf tube separated from the right ventricle, which was kept in another 1.5 ml tube. Heart segments were stored at -80°C until needed. After freezing in liquid nitrogen, heart tissues were grinded. Genomic DNA was isolated by using the gSYNC DNA extraction kit, following the manufacturer's protocol. The NanoDrop spectrophotometer (Thermo Scientific) was used to determine the concentration of the isolated DNA. The mouse sex-determining region *Y* (*SRY*) primers used were forward: 5'- TTT TGC CTC CCA TAG TAT TTC CT -3' and reverse: 5'- TGT ACC GCT CTG CCA ACC A-3'. Each reaction contained 10 µl of 2x SensiFAST SYBR No-ROX Mix, 1 µl of 10x iCycler iQ External Well Factor Solution, 0.8 µl of 20µM *SRY* primers (0.4 µl forward primer, 0.4 µl reverse primer, 200 ng of genomic DNA templated, and sterile molecular biology reagent water to complete a reaction volume of 20 µl. qPCR was performed using the BIORAD iCycler Machine using the following protocol: (i) 40°C/30sec, (ii) 95°C/2min, (iii) 24 cycles of 95°C/15sec, 58°C/15sec, 72°C/15sec, (iv) 95°C/15sec, and (v) 20°C/30sec.

Detection of Glo1 protein

BMCs cultured for 7 days were lysed using RIPA buffer with protease inhibitor (Roche) in order to extract proteins. Equal amounts of protein (50 μg) were loaded into 7% stacking gel and separated in 12% resolving gel. Sodium dodecyl sulfate polyacrylamide gel electrophoresis (SDS-PAGE) was performed at 80V/30 min, and then 120V until totally resolved. Protein was transferred at 70V/1h onto nitrocellulose membranes (Amersham™ Protan™ 0.2μm; GE Healthcare Life Sciences). Membranes were blocked in 5% non-fat dry milk in TBS–Tween 20 buffer for 1h before probing with primary antibodies. Incubation with mouse anti-c-myc tag (9E10, 1:1000), and anti-β-actin (1:5000) antibodies was performed overnight/4°C. Horseradish peroxidase (HRP)-conjugated secondary antibodies (1:1000, Cell Signaling Technology) were incubated for 1h with continuous shaking. Signal detection was performed by enhanced chemiluminescence (ECL) with the SuperSignal™ West Femto kit (Thermo Scientific). ImageJ was used to adjust the contrast and enhance the distinction of bands.

Statistical analysis

Statistical analyses were performed using GraphPad PRISM 5 software. Data is presented as mean ± standard error of measurement (SEM). Unless otherwise specified, comparisons of data between multiple groups were performed by a one-way analysis of variance with a post-hoc Tukey test to establish differences between individual groups, while comparisons between two groups were analyzed using a two-tailed student's t-test. The Grubb's test was used to determine outliers. Statistical significance was given for $p<0.05$.

5. Results

5.1 *Glo*1 expression is reduced after MI

MG Levels have been shown to increase after MI as early as at 6 hours post-infarction with persistence for up to 4 weeks (Blackburn et al., 2017). However, it is unknown whether decreased Glo1 levels or activity, or both, contribute to the accumulation of MG. Therefore, we investigated the expression of endogenous *Glo*1 in the left ventricle scar and border zone tissue after MI in mice. The expression of G*lo*1 was analyzed by RT-qPCR at time-points of 2, 7 and 14 days post-MI in order to aim for the three phases of MI healing: inflammation, proliferation and maturation, respectively. *Glo*1 expression levels were reduced at all time points studied, compared to the healthy control group, but to a different extent. As shown in Figure 5.1, at the first stage (2 days-post MI; n=8), *Glo*1 expression was reduced by 1.68-fold, and during the proliferation stage (7 days post-MI; n=8), levels dropped further to 5.47-fold less compared to healthy tissue ($p<0.05$). Interestingly, during the maturation phase (14 days after MI; n=7), G*lo*1 mRNA levels started to increase, yet remained lower by 2.02-fold in relation to the healthy group. Delta calculations were analyzed by a one-way analysis of variance with a Dunnett's Multiple comparison post-test to compare all time points to the healthy control group.

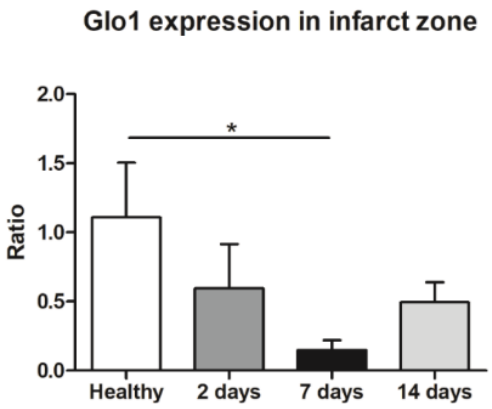

Figure 5.1. Glo1 expression in infarct zone. qPCR analysis of the expression of endogenous *Glo*1 mRNA in the infarct zone of WT mice at 2, 7 or 14 days after MI. The healthy control sample was obtained from the apical area of the myocardium of mice with no MI induced. *Glo*1 expression levels were reduced at all time points post-MI, and by the greatest degree after 7 days. Data is presented as mean ±SEM and analyzed by a one-way analysis of variance with a Dunnett's Multiple comparison post-test using the healthy group as a control (*p<0.05).

Because MG was shown to increase significantly in the heart after MI (Blackburn et al., 2017), the drop in expression of Glo1, the main MG detoxifier, could be set as a causative mechanism. Having identified that *Glo*1 expression is reduced post-MI (this study) and that MG accumulates in the infarcted heart (Blackburn et al., 2017), we next tested our hypothesis that the overexpression of Glo1 could be a potential approach to enhance the survival and therapeutic efficacy of BMCs after injection as therapy to the MI heart.

5.2 Glo1 overexpressing BMCs and mouse model

For this project we used human Glo1 overexpressing mice (Glo1 mice) previously characterized in our laboratory (Blackburn et al., 2017; Vulesevic et al., 2014). Prior to any experiment, mice were genotyped by end-point PCR using primers specific for the transgenic *h*Glo1 gene to distinguish WT mice from Glo1 mice (Figure 5.2).

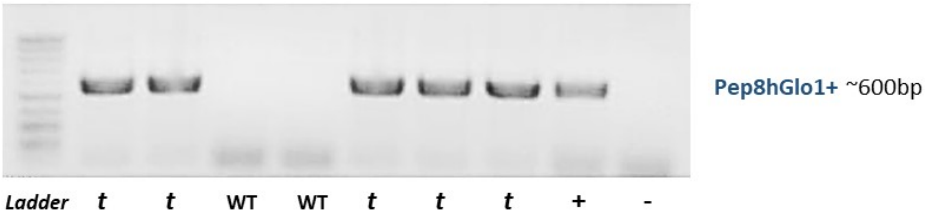

Figure 5.2. Genotyping by End-point PCR. All mice samples positive for amplification of *h*Glo1 (*t*=transgenic) were categorized as Glo1 mice, while all negative samples were classified as WT mice.

Subsequently, BMCs were isolated from bone marrow of both WT and Glo1 mice using Histopaque. After 4-7 days culture, and before using BMCs, the presence of the *h*Glo1 transgenic construct in the isolated BMCs was again screened by end-point PCR (Figure 5.3). Once the presence of the transgene was confirmed, and thus WT BMCs and Glo1 BMCs were obtained, we proceeded with the *in vitro* and *in vivo* experiments.

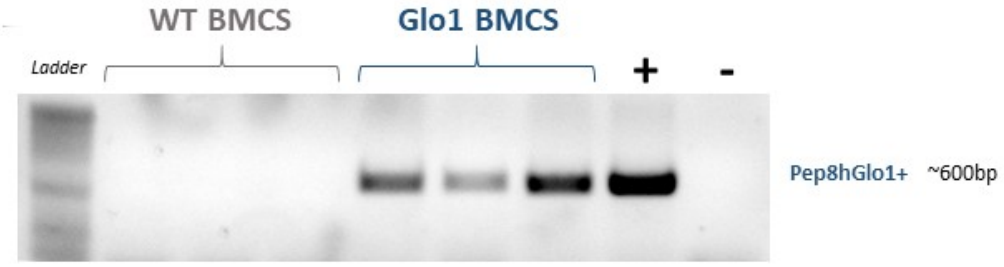

Figure 5.3. Glo1 transgene presence after culture. Genotyping of BMCs cultured for 4-7 days using primers specific for the *h*Glo1 transgene construct.

5.3 MG effects on BMC viability

As multiple studies reported poor BMC survival after transplantation/injection, we first wanted to investigate whether MG is causative to this poor BMC survival due to its cytotoxicity; and if this is the case, can BMCs be protected against MG harmful effects by Glo1 overexpression. To

this end, a Live/Dead assay was used to quantify the survival (percentage) of cells after 24h and 48h exposure to MG. The viability % was determined after 24h exposure to 5µM MG to observe the early effects of MG treatment. Glo1 BMCs exposed to PBS (control) showed a survival rate of 88 ±2.8% (n=4), while PBS-treated WT BMCs (82 ±4.3%; n=4), MG-treated Glo1 BMCs (81 ±2.8%; n=4) and MG-treated WT BMCs (81 ±3.65; n=4) all had similar viability. Overall, viability of both Glo1 overexpressing BMCs and WT BMCs was not significantly affected in any of the groups after 24h exposure to treatment (Figure 5.4).

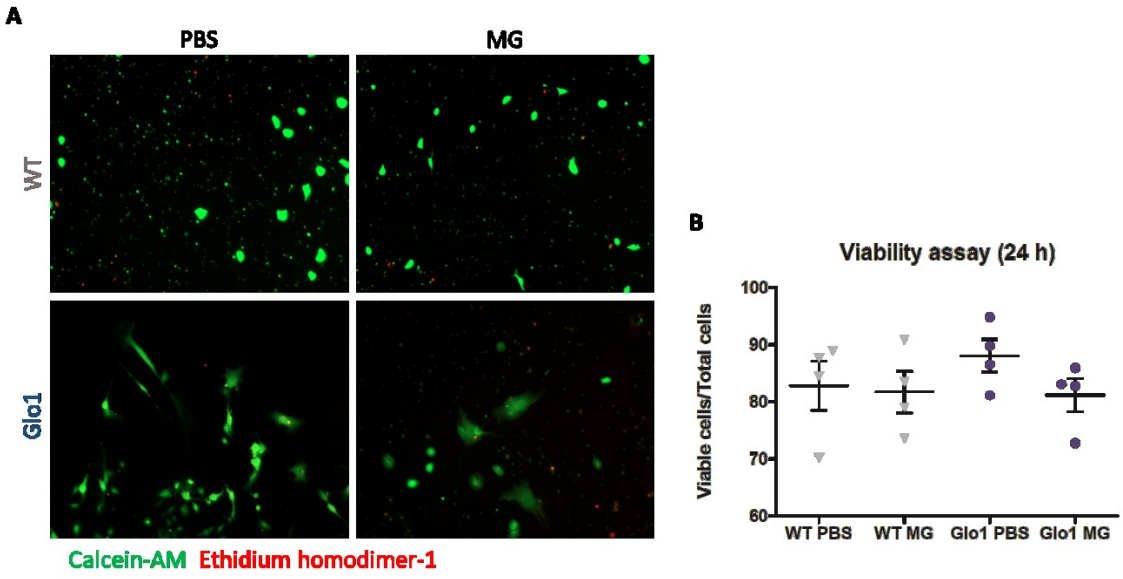

Figure 5.4. Viability assay (24h). (**A**) Microscopy images of WT or Glo1 BMCs treated for 24 hours with 5µM MG or PBS as control. Calcein-AM (green) stained live cells, ethidium homodimer-1 (red) stained dead cells. (**B**) Viability presented as viable cells / total cells. Data are presented as mean +SEM and analyzed using one-way ANOVA with Tukey post-hoc test for multiple comparisons.

Since MG is accumulated in the cells and tissues, we proceeded to evaluate if the exposure for a longer period would have a more pronounced effect on the BMC survival. The viability assay was repeated using a culture period of 48h using the same MG concentration of 5µM (Figure 5.5). After 48h MG treatment, the PBS and MG- treated Glo1 BMCs (n=4) showed a

survival percentage of 75 ±5.8% and 75 ±5.4%, respectively, while both WT groups (n=5) displayed a similar viability rate of 72 ±2.4% and 72 ±4.5%, respectively. Comparing the relative change between MG treatment vs control (Figure 5.5C), Glo1 BMCs displayed a similar tolerance against MG compared to their WT counterpart. After normalizing all values of the 24h and 48h experiments to the 24h PBS-treated WT group, the viability of both Glo1 BMCs and WT BMCs was not significantly affected in any of the groups (Figure 5.5D).

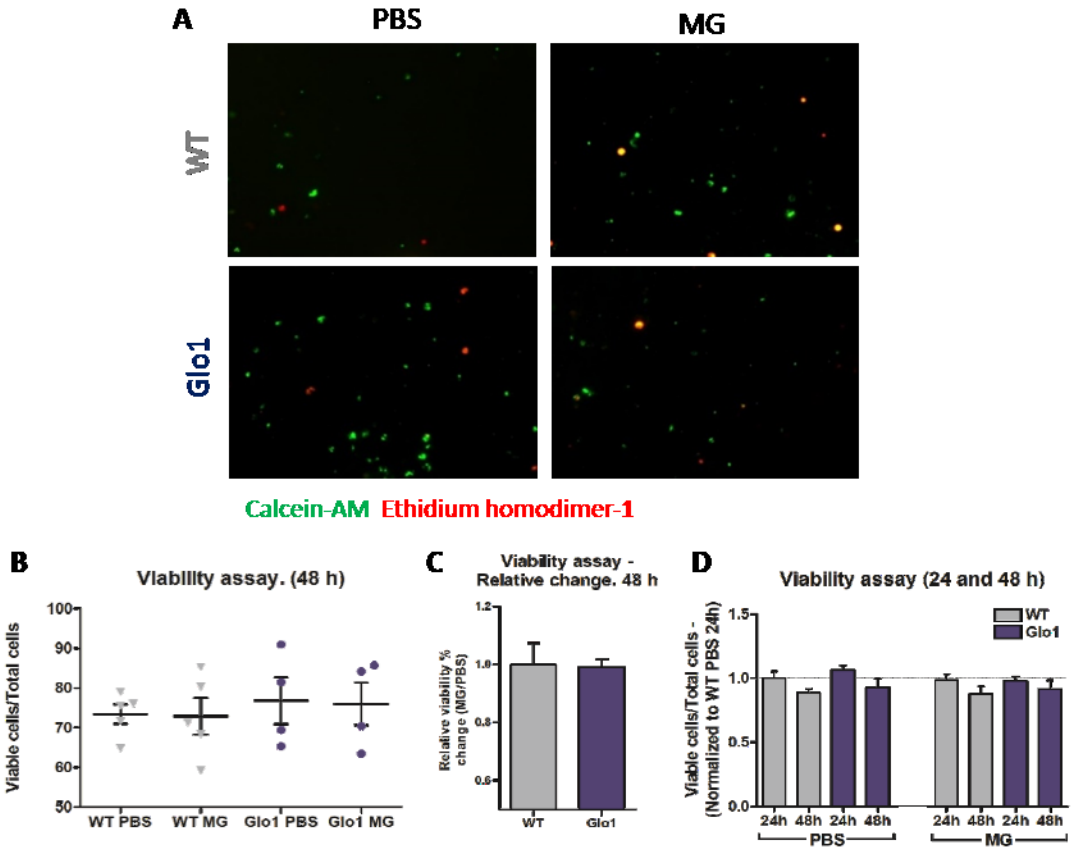

Figure 5.5. Viability assay (48h). (**A**) Microscopy images of Glo1 or WT BMCs treated for 48 hours with 5 µM MG or PBS as control. Calcein-AM (green) stained live cells, ethidium homodimer-1 (red) stained dead cells. (**B**) Viability presented as viable cells / total cells. (**C**) Relative change in viability % (MG/PBS). (**D**) % Viability after 24h (n=4) and 48h (n=4) presented as viable cells / total cells, normalized to % viability of WT PBS-24h. Data are presented as mean +SEM. (**B, D**) analyzed using one-way ANOVA with Tukey post-hoc test for multiple comparisons, and (**C**) analyzed using student's two-tailed t-test.

5.4 Intracellular ROS production is increased post-MG treatment

Next, we investigated the effect of MG on the formation of oxidative stress in Glo1 and WT BMCs. To analyze this, intracellular ROS content was measured using a cell-permeable dye that, after reacting with ROS, generates a red fluorescent signal (Ex/Em=650/675 nm). ROS production was compared between Glo1 BMCs (n=5) and WT BMCs (n=5) after 24 hr treatment with one of the following: A) PBS, as negative control, B) 5µM MG, and C) 10µM H_2O_2 as positive control. Relative fluorescence of WT BMCs was higher in all treatments, especially in the negative control (PBS), compared to the PBS-treated Glo1 group (Figure 5.6). Production of ROS tended to increase in WT BMCs exposed to PBS (p=0.110) and to H_2O_2 (p=0.103). Notably, exposure to MG resulted in a significantly higher (p<0.05) production of ROS by WT BMCs, compared to Glo1 group.

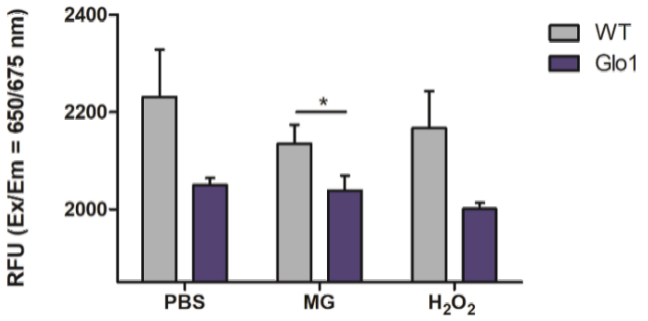

Figure 5.6. Glo1 overexpression can reduce the intracellular ROS production of BMCs treated with MG. $4x10^4$ WT or Glo1 BMCs were cultured on fibronectin coated wells and treated for 24h with: PBS, 5µM MG or 10µM H_2O_2 (n=5 for each). Fluorescence was read at Ex/Em=650/675 nm and expressed in relative fluorescence units (RFU). Data are presented as mean ±SEM and analyzed using student's two-tailed t-test to compare between WT and Glo1 groups for each treatment (*p<0.05).

5.5 Superoxide dismutase (SOD) production is reduced after treatment with MG

The next study aimed to determine if SOD activity is reduced in BMCs due to the presence of MG, and whether Glo1 overexpression has the potential to prevent this SOD reduction. After 24h treatment with ±5μM MG, proteins from Glo1 and WT BMCs (n=5, each) were isolated and SOD content was quantified using a colorimetric assay kit. Glo1 BMCs showed significantly higher SOD production compared to WT group after exposure to PBS (p<0.05; Figure 5.7A). Figure 5.7B shows the relative levels of O_2^- produced by each treatment condition normalized to PBS-treated WT BMCs. WT BMCs produced more oxidative stress in the presence of PBS compared to Glo1 BMCs (p<0.05). These results suggest a higher resistance against oxidative stress provided by overexpression of Glo1.

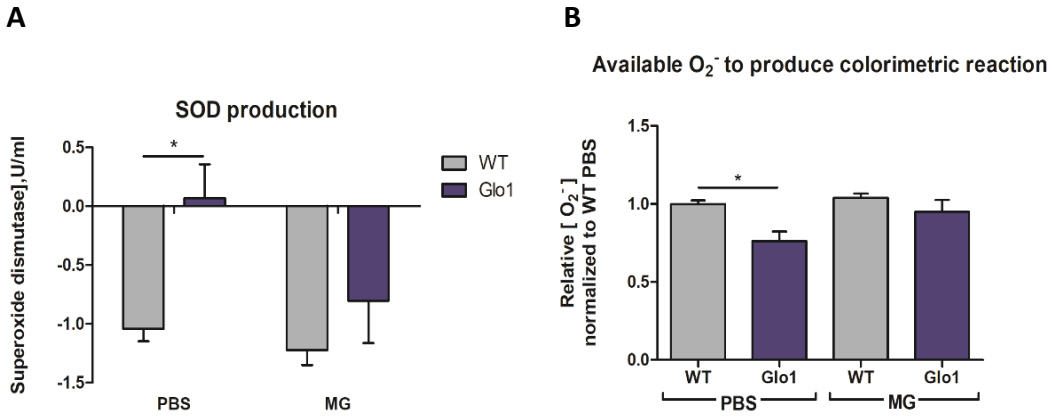

Figure 5.7. Superoxide Dismutase (SOD) assay. The loss of SOD levels is minimized by Glo1 overexpression. After 24h treatment with ±5μM MG, 2x10^5 WT and Glo1 BMCs (n=5) were harvested and proteins isolated using cold lysis buffer. Using a superoxide dismutase assay kit, absorbance at OD= 440nm was read immediately and 60 min later. (**A**) Normalized readings were plotted in the graph to obtain SOD production in U/ml. (**B**) Available O_2^- to produce colorimetric reaction. More colour produced indicates less SOD available to scavenge O_2^-. Data are presented as mean ±SEM and analyzed using student's two-tailed t-test to compare between groups (*p<0.05).

5.6 *In vitro* angiogenic potential of BMCs after MG treatment

BMCs have been shown to have pro-angiogenic effects and MG has been demonstrated to decrease this property (Dobler et al., 2006). This project aimed to confirm the detrimental effect of MG on BMC pro-angiogenic properties and to evaluate if Glo1 overexpression would reverse this effect. For this reason, the angiogenesis assay with HUVECs was used to assess the ability of BMCs to promote vascular structure formation from HUVECs. WT and Glo1 BMCs were exposed for 24h to ±5µM MG prior to *in vitro* ECMatrix assay, and then co-cultured with HUVECs.

For the first analysis of the angiogenesis assay (Figure 5.8), total network length was measured in millimeters. HUVECs cultured alone (n=10) yielded a network length of 71.96 ±5.6 mm. In co-culture with 5µM MG-treated WT BMC (n=5), HUVECs showed a significant reduction in formation of vessel-like structures (58.32 ±11.08 mm) compared to the PBS-treated WT group (79.60 ±8.26 mm; $p<0.05$). On the other hand, HUVECs combined with PBS-treated Glo1 BMCs (n=6) yielded a formation of vessel-like structures (91.29 ±4.88 mm) that was preserved when Glo1 BMCs were exposed to 5µM MG (73.35 ±9.02 mm) (Figure 5.8B), thus showing a possible protective effect of Glo1 overexpression against the anti-angiogenic effects of MG.

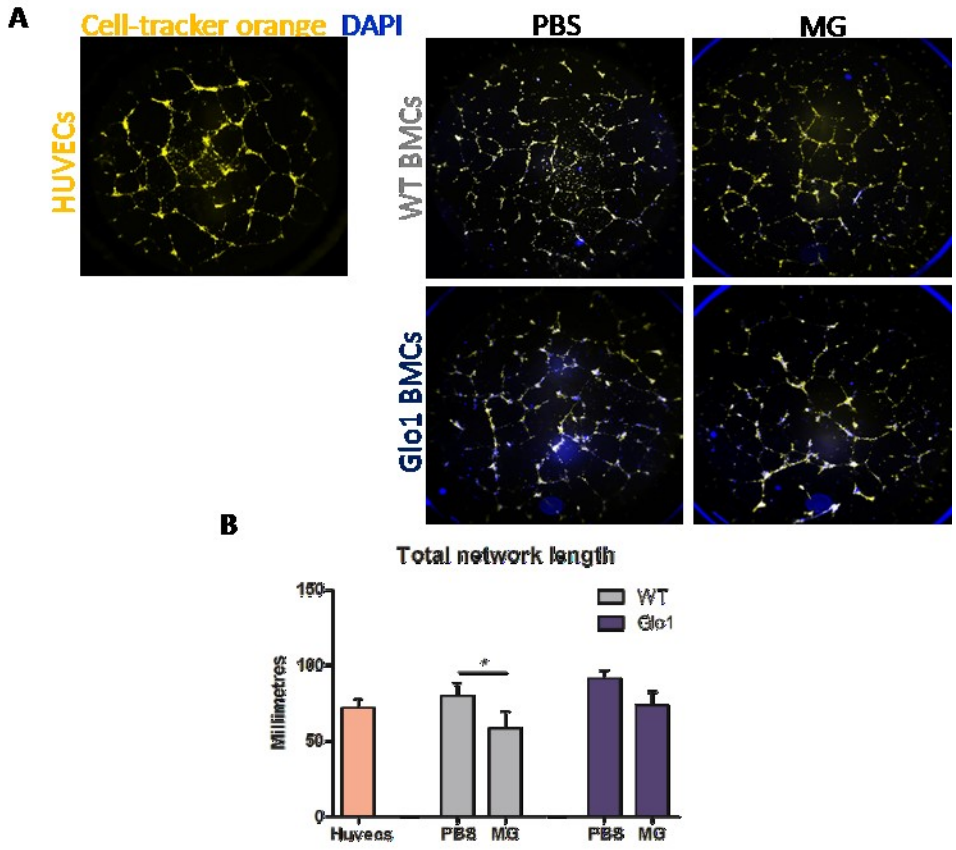

Figure 5.8. Angiogenesis assay. MG impairs formation of network-like structures. (A) Microscopy images (1.25X magnification) of total tubule length of: HUVECs (n=10), HUVECs co-cultured with PBS-treated WT BMCs (n=5), HUVECs co-cultured with 5µM MG-treated WT BMCs (n=5), HUVECs co-cultured with PBS-treated Glo1 BMCs (n=6), and HUVECs co-cultured with 5µM MG-treated Glo1 BMCs (n=6). BMCs were stained with DAPI, and HUVECs were stained with Celltracker orange**. (B)** Measurement of total network length expressed in millimeters. Data are presented as mean ± SEM and analyzed using student's two-tailed t-test to compare between groups (**p*<0.05)**.**

In the angiogenesis assay, the ability of BMCs to contribute to the formation of HUVECs cellular network was also assessed (Figure 5.9). The number of $DAPI^{+}$ BMCs present in HUVECs network structure formation ($Cell\text{-}tracker^{+}$) was quantified by FOV (n=3) (Figure 5.9A, B). There was a trend for a reduced number of MG-treated WT BMCs incorporating into vessel-like structures (n=5; 140.6 ±29.6) compared to the PBS-treated WT BMCs (n=5; 199.06 ±24.41;

p=0.09). For Glo1 BMCs, those treated with MG showed a preserved ability to incorporate into capillary-like networks (n=4; 140.3 ±17.3) compared to the PBS-treated group (n=4; 163.29 ±29.3) (Figure 5.9B). This result was further supported after normalizing the number of cells treated with MG by dividing them with their corresponding control (MG/PBS; Figure 5.9C). Here, Glo1 BMCs demonstrated a significantly superior preservation of their capacity to incorporate into the tubular structures compared to their counterpart WT group after MG treatment (*p*<0.05).

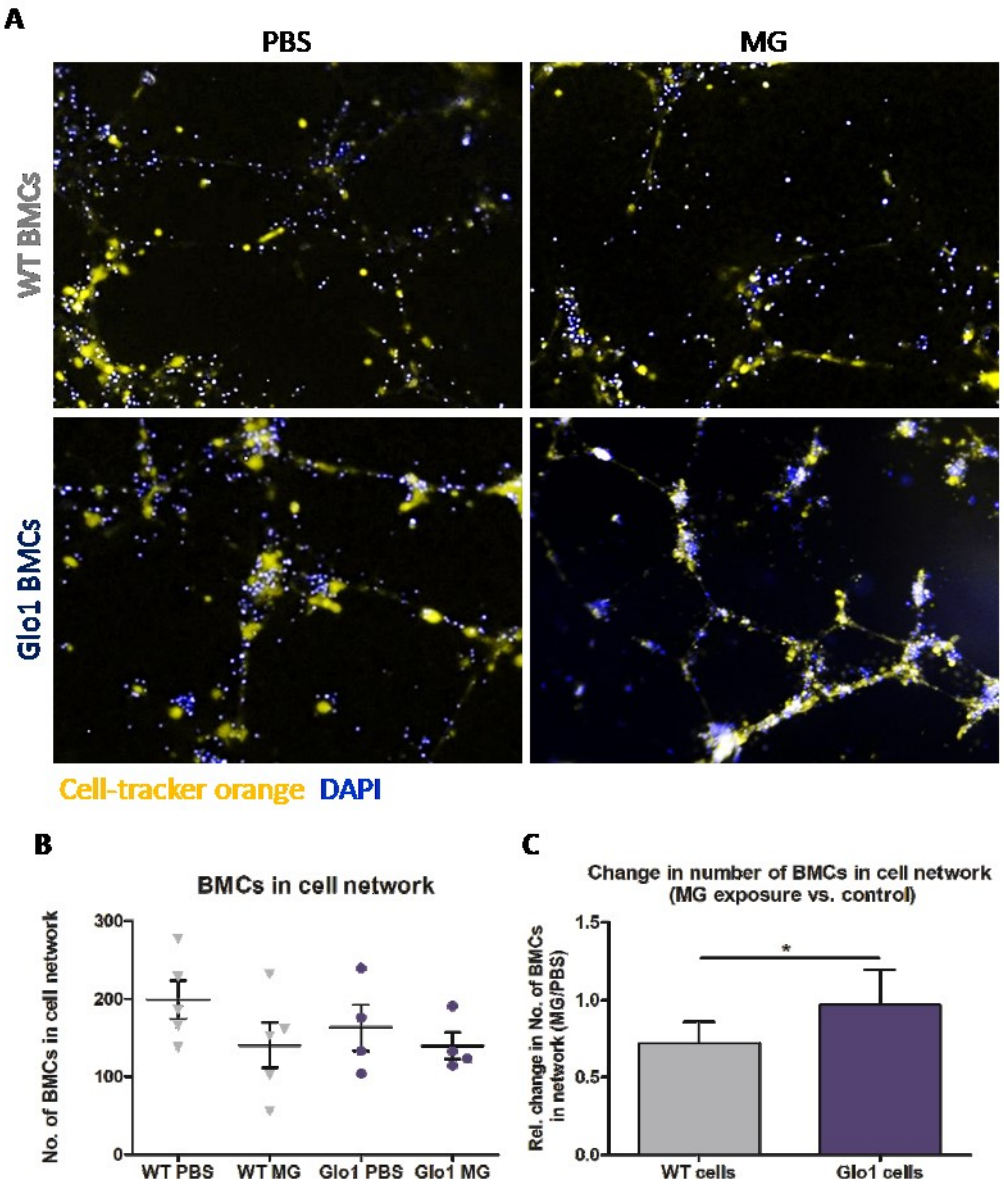

Figure 5.9. Angiogenesis assay. MG impairs incorporation of BMCs into vessel-like structures. **(A)** Microscopy images (1.25X magnification) of ECMatrix angiogenesis assay with: HUVECs co-cultured with PBS-treated WT BMCs (n=5), HUVECs co-cultured with 5µM MG-treated WT BMCs (n=5), HUVECs co-cultured with PBS-treated Glo1 BMCs (n=6), and HUVECs co-cultured with 5µM MG-treated Glo1 BMCs (n=6). BMCs stained were with DAPI, and HUVECs were stained with Celltracker orange. **(B)** Quantification of DAPI+ BMCs contributing to structure formation per FOV (n=3, 1.25X magnification). **(C)** Relative change in number of BMCs contributing to capillary-like network (MG/PBS). Data are presented as mean ± SEM and analyzed using student's two-tailed t-test to compare between groups (*p<0.05).

5.7 Chemo-attractant properties of BMCs treated with MG

The pro-angiogenic properties of BMCs are largely due to the paracrine factors that they produce (Arnous et al., 2012). We therefore proceeded to evaluate the effect of MG exposure on the ability of the supernatant of BMCs to induce migration of endothelial cells. To assess this, a vertical chemotaxis migration assay was performed. On this test, HUVECs were loaded into the upper chamber and allowed to migrate overnight towards one of the following chemo-attractants in the lower chamber: conditioned media from WT or Glo1 BMC cultures ±5μM MG, complete M200 media or serum/growth factor-free M200 media. Conditioned media from WT BMCs exposed to PBS attracted 3.1 ±1.5 HUVECs/FOV, while in exposure to MG it attracted 3.6 ±2 cells/FOV. On the other hand, the supernatants of the Glo1 BMC cultures exposed to PBS or MG were able to attract 5.5 ±1.6 and 5.2 ±1.7 HUVECs/FOV, respectively. Overall, no difference was observed in the chemo-attractant properties of WT and Glo1 BMCs conditioned media (Figure 5.10B).

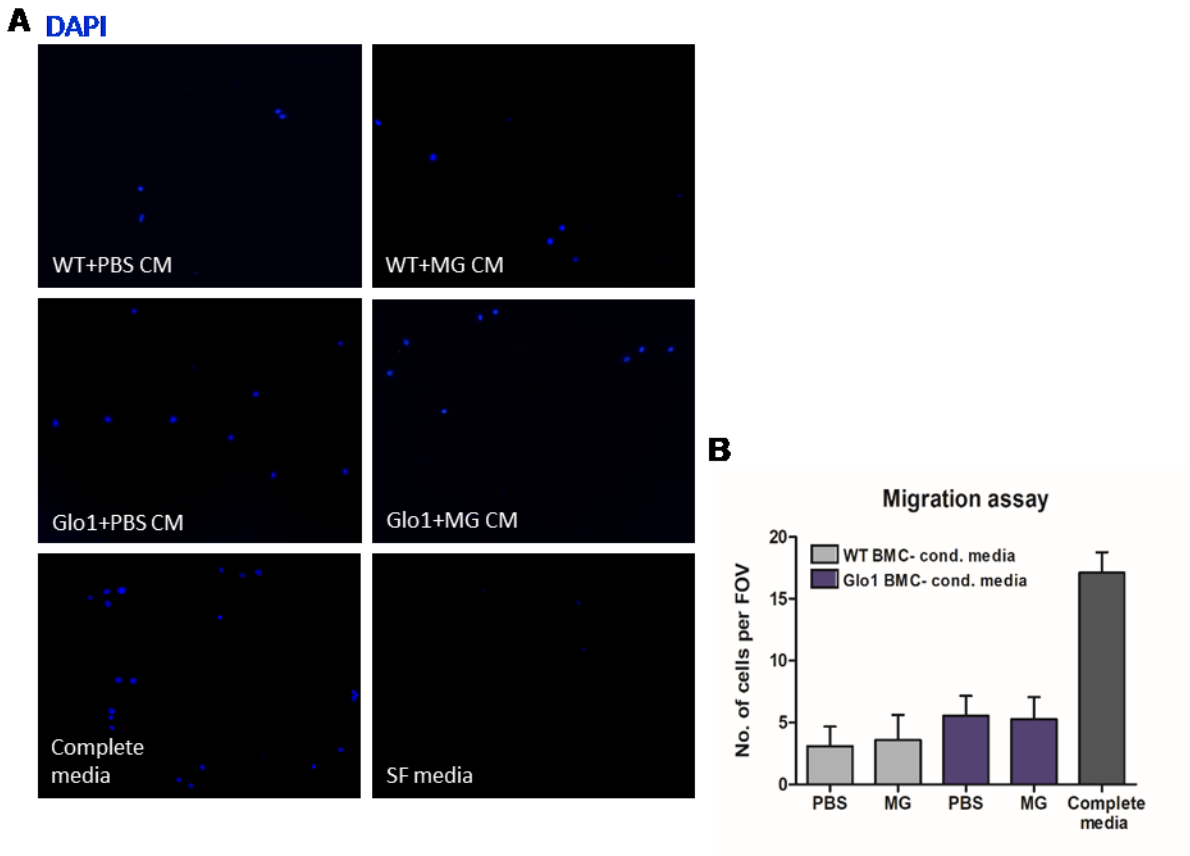

Figure 5.10. Migration assay. 2x10^4 HUVECs were cultured in the upper chamber and allowed to migrate overnight towards one of the following media: conditioned media of WT BMCs ±5µM MG (n=6), CM of Glo1 BMC ±5µM MG (n=6), complete M200 media (n=6), or serum/growth factors-free media (n=6). Cells were then fixed, stained with DAPI and imaged under fluorescence microscopy, ×10 magnification. (**A**) Representative microscopy images of migrating HUVECs towards chemo-attractant. (**B**) Graph showing the number of migrating cells counted per field-of-view (FOV) (n=3). Migration towards complete media is used as a control and reference. Data are presented as mean ±SEM and analyzed using one-way ANOVA with Tukey post-hoc test for multiple comparisons.

Based on the *in vitro* results of this study, Glo1 overexpression appears to improve the function of BMCs in the presence of MG, making this a potential approach for pre-conditioning cells for use in treating myocardial infarction. To assess this hypothesis, MI-induced WT mice received one of the following treatments into the infarct border zone: PBS as control, 3.5x10^5 WT BMCs,

or $3.5x10^5$ Glo1 BMCs. Then, their potential to improve MI healing was determined by assessing cardiac function, cardiac scar size and the formation of vessels in the infarct and border zones.

5.8 Cardiac function

Assessed by echocardiography, cardiac function was determined before treatment injection (baseline, 7 days post-MI) and at 21 days post-treatment (end of study, 28 days post-MI) (Figure 5.11A). LVEF and FAC percentages were compared between the three treatment groups at both time points. Both BMC-treated groups (WT (n=8) and Glo1 (n=7)) and the PBS-treated mice (n=6) showed maintenance in %LVEF over time. The WT BMC group went from 39.2 ±2.1% to 41.6 ±2.1%, the Glo1 BMC group went from 40 ±1.7% to 37.8 ±2, and the PBS-treated group went from 41.2 ±2.2% to 36.9 ±3.2%. (Fig 11B). FAC percentage was also conserved at the end of the study compared to baseline in all treatments. WT BMC-treated group went from 25.6 ±1.1% to 27.5 ±2.1%, Glo1 BMC-treated mice went from 24.9 ±1.1% to 24.2 ±1.1%, while PBS-treated group went from 25.1 ±1.4% to 23 ±1.9%) (Figure 5.11C). In addition, there was no statistical difference between treatment groups, when analyzing the relative change in %LVEF and %FAC between baseline and end-of-study (Figure 5.11D and 5.11E, respectively).

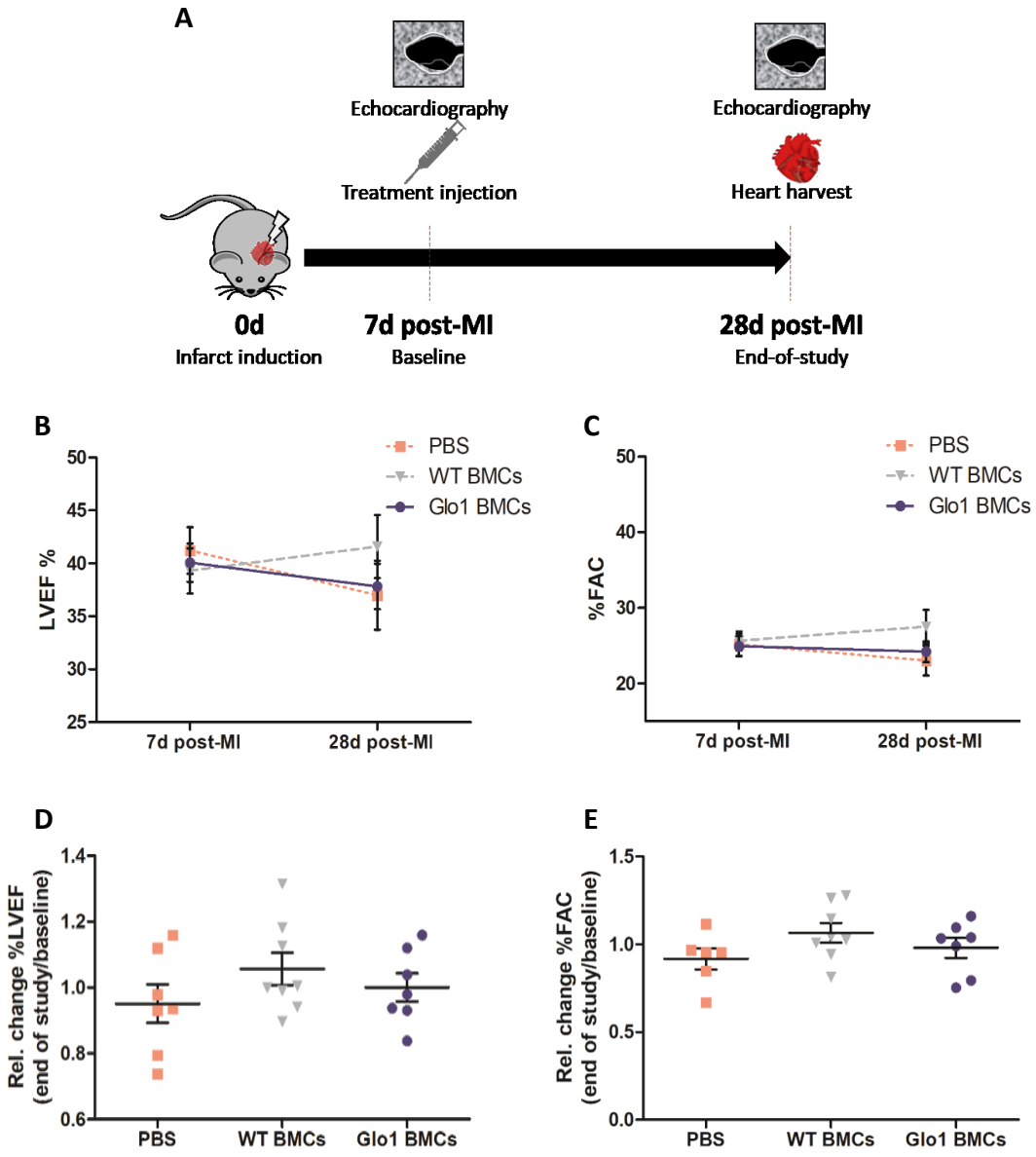

Figure 5.11. Cardiac function. (**A**) Schematic representation of timing used for delivery of treatment (PBS, WT or Glo1 BMCs) via injection at 7 days after MI induction (baseline) and harvest of the hearts at day 28 post-MI (end-of-study). Echocardiography was assessed at both time points. Echocardiography assessment of (**B**) left ventricular ejection fraction (%LVEF), and (**C**) fractional area change (%FAC), at baseline and end-of-study. (**D**) Relative change of %LVEF between baseline and end-of-study. (**E**) Relative change of %FAC between baseline and end-of-study. Treatments for WT mice included one of the following injections: PBS control (n=6), 3.5 x10^5 WT BMCs (n=8), or 3.5 x10^5 Glo1 BMCs (n=7). Data are presented as mean ± SEM and analyzed using one-way ANOVA with Tukey post-hoc test for multiple comparisons.

5.9 Infarct area and fibrosis

Hearts harvested at the end of study were snap frozen, sectioned and stained using Masson's trichrome staining to identify the blue collagenous scar and the red muscle tissue. Scar length/total heart length was used to measure the scar size. PBS and WT BMC-treated groups exhibited scar sizes of 33.35 ±2.9% and 34.52 ±1.8%, respectively; while the Glo1 BMC-treated group had a scar size of 34.04 ±3.7%. Overall, no difference in relative scar formation was observed between any of the treatments (Figure 5.12).

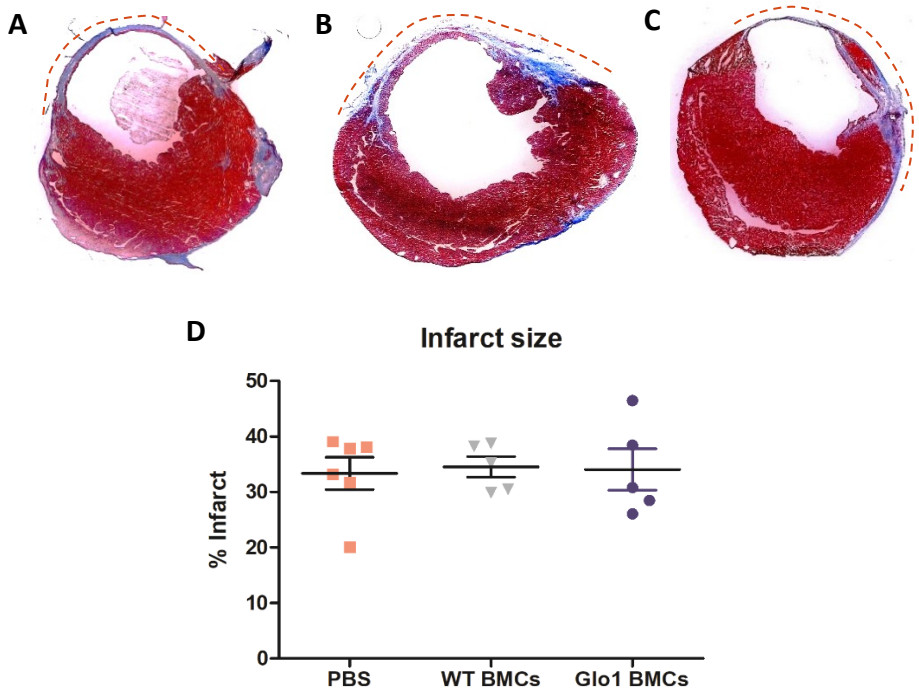

Figure 5.12. Infarct size and fibrosis formation. (**A-C**) Representative images of cross-sectioned Masson's Trichrome Stained hearts at end of study (21 days after treatment) showing infarct area in the left ventricle (segmented, blue line) and fibrosis formation caused by MI induction. The blue colour identifies the collagenous scar, and the red is muscle tissue. (**A**) PBS treated MI heart (n=6), (**B**) WT-BMC treated MI heart (n=5), (**C**) Glo1-BMC treated MI heart (n=5). (**D**) Percentage of infarct area with respect to total heart area in all treatments. Data are presented as mean ±SEM and analyzed using one-way ANOVA with Tukey post-hoc test for multiple comparisons.

5.10 Vascular growth induction

In order to evaluate neo-vessel formation, heart sections were also immunostained with α-SMA and CD31/PECAM antibodies to label arterioles and capillaries, respectively, in the infarct and peri-infarct zones. Positively stained structures were counted per FOV (n=3) in a blinded fashion. Structures positively labelled for α-SMA^{+} and CD31^{+} were more prevalent at the border zone than in the infarct zone of all groups. All groups displayed similar number of arterioles in the infarct zone (PBS=11.5 ±1.2, WT=12.1 ±1.6, Glo1=12.2 ±1.4) and in the peri-infarct zone (PBS=14.6 ±1.7, WT=16. 5 ±2.8, Glo1=14.6 ±2.8) (Figure 5.13B). On the other hand, the number of CD31^{+} structures in the infarct zone (Figure 5.13C) was slightly higher in both cell-treated groups (Glo1=105.7 ±9.8, WT=99.13 ±11.1) with respect to the control (PBS=86.1 ±14.5). Compared to control group (PBS=125.5 ±19.1), capillaries in the border-zone tended to be more abundant in the Glo1 BMC-treated group (p=0.133, 182.2 ±12.1) and were significantly more numerous in the WT BMC-treated set (p<0.005, 195.8 ±22.3) (Figure 5.13C). These results showed that treatment with WT or Glo1 overexpressing BMCs may lead to an improvement in the formation of vessels in the area surrounding the infarction.

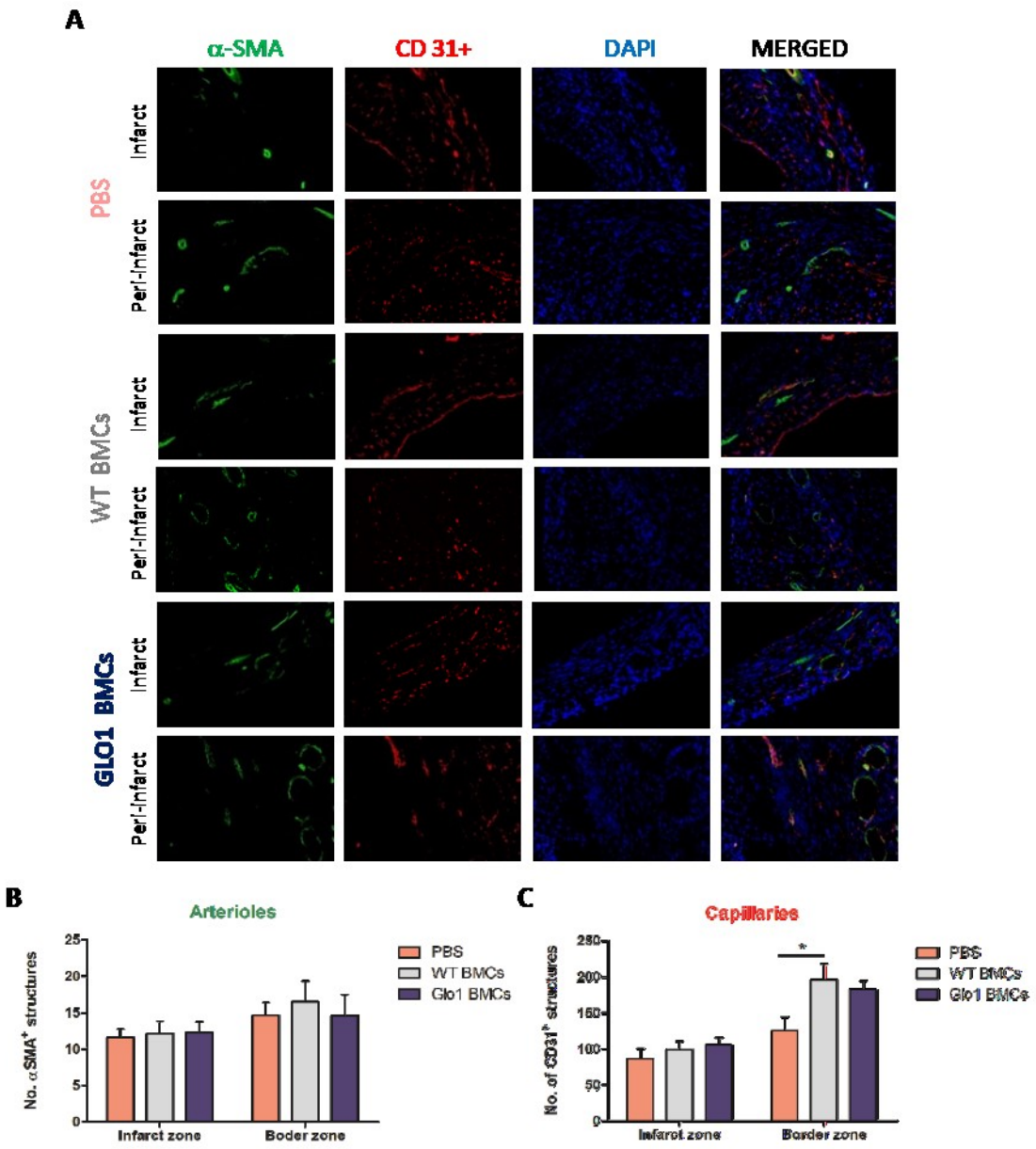

Figure 5.13. Immunostaining of vascular structures. (**A**) Representative images of α-SMA (arterioles) and CD31/PECAM (capillaries and endocardium) double-immunostained infarct and peri-infarct zones of cross-sectioned MI mice hearts treated with PBS (n=6), WT BMCs (n=5) or Glo1 BMCs (n=5). (**B**) Number of α-SMA+ and (**C**) CD31+ structures at the infarct and peri-infarct zone counted per field-of-view (n=3) in a blinded fashion (*p<0.05). Data are presented as mean ±SEM and analyzed using one-way ANOVA with Tukey post-hoc test for multiple comparisons.

5.11 Detection of transplanted BMCs in the infarct area

Given the little to no improvement in cardiac repair and function observed *in vivo* with Glo1 BMCs treatment, we wanted to know whether Glo1 overexpression was affecting the retention of BMCs after 3 weeks of injection. For this, WT and Glo1 BMCs from male mice were injected in the hearts of female infarcted mice and 21 days later, hearts were harvested. Then, genomic DNA was isolated from infarct and border zone together, keeping the right ventricle as an internal control. *Y* chromosome was detected by qPCR, using DNA isolated from the heart of a male mouse as a positive control. After 3 weeks of injection, the *Y* chromosome could not be detected in any of the treated mice, whether they were treated with Glo1 or with WT BMCs (Figure 5.14). Thus, BMCs did not survive *in vivo* and may explain, in part, why we did not see any changes in cardiac function.

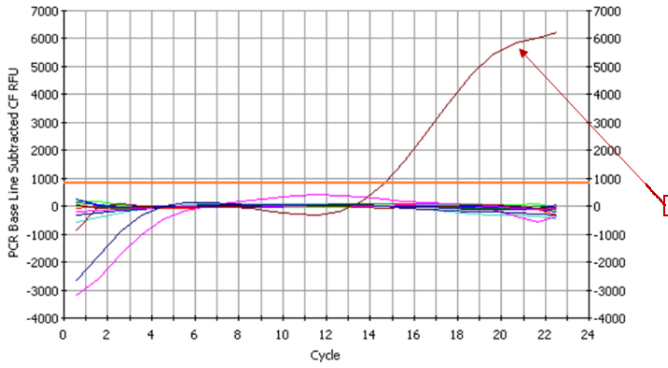

PCR Quantification Spreadsheet Data for FAM-490

Well	Identifier	Ct
A01	Glo1-BMC treated mouse (infarct/border zone)	N/A
A02	WT-BMC treated mouse (infarct/border zone)	N/A
A03	Glo1-BMC treated mouse (infarct/border zone)	N/A
A04	WT-BMC treated mouse (infarct/border zone)	N/A
A05	WT-BMC treated mouse (infarct/border zone)	N/A
A06	Glo1-BMC treated mouse (infarct/border zone)	N/A
A07	Male mouse (+ control)	14.6
A08	- control	N/A
B01	Glo1-BMC treated mouse (Right ventricle)	N/A
A02	WT-BMC treated mouse (Right ventricle)	N/A
A03	Glo1-BMC treated mouse (Right ventricle)	N/A
A04	WT-BMC treated mouse (Right ventricle)	N/A
A05	WT-BMC treated mouse (Right ventricle)	N/A
A06	Glo1-BMC treated mouse (Right ventricle)	N/A

Figure 5.14. *Y* chromosome detection. To detect the retention of donor BMCs 21 days post-injection, *Y* chromosome was detected by qPCR in tissue isolated from the infarct plus border zones from infarcted female hearts treated with cells of male origin, using their right ventricle as internal negative control. qPCR showed no detection of *Y* chromosome in any of the treated mice. Detection of *Y* chromosome from the male mouse heart (red arrow) was used as control and reference.

5.12 hGlo1 expression in cultured Glo1 BMCs.

As no difference was seen in the *in vivo* therapeutic potential between WT and Glo1 BMCs, we wanted to investigate whether this could be explained by loss of Glo1 transgene expression over time. We thus evaluated whether transgene expression was still preserved after 7 days of BMC culture (which corresponds to the time at which BMCs are lifted from culture for transplantation). The expression of hGlo1 was assessed using Western Blot probed against c-myc tag (used to identify hGlo1). The results demonstrated that the BMCs, previously characterized in our lab right after isolation (Vulesevic et al., 2014), do have preserved Glo1 expression after 1 week of *ex vivo* expansion (Figure 5.15).

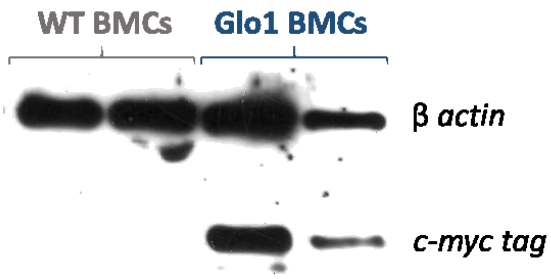

Figure 5.15. Cultured Glo1 BMCs preserve expression of transgenic hGlo1. Proteins from WT and Glo1 BMCs expanded *ex vivo* for 7 days were isolated and quantified. 50µg protein were loaded in SDS-PAGE and transferred to a nitrocellulose membrane. Western blot was probed against c-myc-tagged hGlo1, β-actin was used as control.

6. Discussion

Several studies have assessed the effect of Glo1 overexpression to reduce MG accumulation and prevent diabetic cardiomyopathies and other complications associated with diabetes (Ahmed et al., 2008; Berner et al., 2012; Brouwers et al., 2011, 2016; Shinohara et al., 1998; Vulesevic et al.,

2014, 2016). However, to our knowledge, only our lab has explored the role of MG in the pathogenesis of non-diabetic-related MI and the protective effect of Glo1 overexpression. Blackburn et al. showed that MG-AGEs were increased in the heart post-MI and that overexpressing Glo1 could reduce MG-AGE levels and improve cardiac function (Blackburn et al., 2017). Given that MG accumulates post-MI, this may be a reason why therapeutic cells experience low retention and viability when transplanted to the MI heart, thus limiting their efficacy. Therefore, in this study, we aimed to determine if overexpressing Glo1 in BMCs could improve their function upon exposure to MG, and to see if this would improve their retention and therapeutic potential for treating the MI mouse heart.

We first set out to investigate the expression of Glo1 in the heart after MI. One of the new findings of this work is that Glo1 expression is reduced after MI in the infarct and peri-infarct zones of the heart as early as 2 days and this reduction is maintained for up to at least 14 days. The lowest Glo1 concentration was observed at 7d post-MI, which coincides with the proliferation stage of infarct evolution (Frangogiannis, 2006). Previous studies showed that Glo1 is decreased under conditions of hypoxia, ischemia and inflammation (Rabbani et al., 2016), and in the infarcted heart, MG-AGEs increased by 56% at 6h-post MI which persisted for 4 weeks (Blackburn et al., 2017). The decrease of Glo1 expression might be associated with oxygen availability in the heart, since O_2 is a major determinant of cardiac gene expression (Giordano, 2005). In response to the lack of oxygen, the mitochondria generate ROS which act as a signal for gene transcription regulation by the hypoxia-inducible factor 1 alpha (HIF-1α) (Guzy et al., 2005). In turn, this transcription factor regulates the expression of genes related with angiogenesis, apoptosis and inflammation to heal the heart (Giordano, 2005). On top of that,

HIF-1α has also been associated with Glo1 downregulation in cancer studies (Rabbani et al., 2016).

Because cell therapies have not shown themselves as promising as expected, several studies have proposed cell pre-conditioning as a strategy to improve their robustness prior to their delivery to the post-infarction environment (X. Li et al., 2016). The overexpression of cytoprotective genes in order to improve the survival and retention of post-transplantation cells is one such suggested approach (Arnous et al., 2012). Glo1 overexpressing mice have already been shown to heal better after MI as exhibited by preserved cardiac function and ventricular geometry, increased vasculogenesis and reduced scar formation (Blackburn et al., 2017). For these reasons, this study also examined the ability of Glo1 overexpression to improve the therapeutic benefit of BMCs in a murine MI model. Coinciding with the time-point post-MI in which we detected the lowest Glo1 expression, the transplantation of BMCs to the infarcted hearts was performed at 7 days post-MI. Additionally, this time of delivery is considered appropriate since it is after the acute inflammation found during the first phase but before the maturation of the scar, both of which negatively affect transplanted cell retention and function (Kanda & Davis, 2017).

LVEF and FAC values were used to evaluate post-MI cardiac function and as exclusion criteria. This study only included those infarcts with LVEF within the range {28.76% - 50.74%} after 7-days of MI. Despite this, the baseline values of LVEF in this study can be considered to be inconsistent, and thus the therapeutic effect of any of the treatments could have been masked. Therefore, the relative change (end of study/baseline) in LVEF and FAC was determined in addition to the absolute values to minimize the effect of variability between mice. No significant differences were seen between the treatments with WT or Glo1 BMCs or PBS; nor

were there differences observed when analyzing the relative change. As the tissue remodelling and scar extension correlates with FAC and LVEF (Kanno et al., 2002), the scar size was also compared between treatments; however, the same variability between samples was found. This inconsistency in the size and severity of the infarcts might have resulted from artifacts caused during the surgery. In addition, the ventricular apex becomes poorly visible when damaged, making the correct tracing of the endocardial border more difficult (Benavides-Vallve et al., 2012). Thus, I may have experienced some technical issues in making the assessment of cardiac scar and function.

This study did not find a significant difference in infarct size or cardiac function in the groups treated with WT or Glo1 BMCs compared to PBS. A similar result was found in another study that overexpressed endothelial nitric oxide synthase (eNOS) in BMCs to treat MI in pigs (Ward et al., 2013). However, many studies with BMCs overexpressing other protective genes have shown an improvement in the therapeutic response after MI (J. Cho, Zhai, Maejima, & Sadoshima, 2011; Duan et al., 2003; L. Li et al., 2013). While these studies used at least $1x10^6$ cells, only $3.5x10^5$ cells were injected per heart in this study. The inaccessibility of enough Glo1 mice as well as technical issues in the cell isolation and culture resulted in an insufficient number of BMCs to use more per treatment. This may be an important limitation in this study since the effect of cell therapy has been reported to be cell-number dependent (Mangi et al., 2003). Additionally, it has been shown that the effectiveness of the cell uptake in the peri-infarct zone is determined by the infarct size in response to the gradient of chemoattractants released by the myocardium after ischemia (Musialek et al., 2013). The long-term retention of transplanted cells is restricted to only 1-2% of the injected cells since mechanical washout removes most of them and the few that survive die by apoptosis within 4 days due to the toxic

post-MI environment (Kanda & Davis, 2017). Consistent with the literature, our Y chromosome study showed the absence of male donor BMCs in female infarcted hearts after 21 days of injection, perhaps also contributing to the lack of differences between the groups.

Glo1 BMC therapy coupled with biomaterials such as injectable hydrogels, cardiac patches and microcapsules could help improve their viability and engraftment after delivery in the heart (Kanda & Davis, 2017). Although the biomaterial approach has not directly addressed the effects of MG in the post-MI environment, many different biomaterials have been shown to increase transplanted cell retention, viability and function leading to improved cardiac function post-MI (as reviewed in (Kanda & Davis, 2017; Rane & Christman, 2011)). For example, intra-myocardial injection of hydrogel microcapsules supplemented with matrix proteins enhanced CSCs' viability and long-term retention for 21 days by providing them with anchorage sites, while improving their ability to repair damaged myocardium (Mayfield et al., 2014).

As low survival is one of the limitations of cardiac cell therapy, the effect of 5μM MG on BMCs' viability was evaluated. Our results showed no significant difference between WT and Glo1 BMCs after 24h or 48 h of MG exposure. Another study used higher concentrations of MG, from 10μM to 100μM in endothelial cells and did not observe an effect on viability either (Liu et al., 2012). On the contrary, a previous study from our lab (Vulesevic et al., 2016) exposed BM-derived macrophages and endothelial cells to 5μM MG for 72h and 24h, respectively, and obtained a preservation of viability in the Glo1-overexpressing group compared to their WT counterpart. Differences in the results may be due to cell type specificity. Alternatively, the approach used to obtain Glo1 overexpression might explain this discrepancy. While Vulesevic et al. used plasmid transfection in cells once they were isolated, the present study used BMCs extracted from transgenic mice that constitutively expressed hGlo1. To determine if the

production of hGlo1 is reduced/lost by the culture of Glo1 BMCs for 4-7 days, its expression was verified. We showed that 7 days of *ex vivo* expansion did not silence the production of our transgenic enzyme.

BMCs have been reported to respond to stimulus and migrate to the infarcted heart, where they play an important role in vascular repair (Fadini et al., 2012; Fazel et al., 2006). One of the effects observed in BMC-based therapies is the stimulation of angiogenesis. However, it has been shown that MG can impair the formation of new vessels in diabetic cardiomyopathy (Dobler et al., 2006) and MG-protective overexpression of Glo1 has been related to greater vascular density in an infarcted mouse model (Blackburn et al., 2017). Although the presence of injected BMCs in the heart is transient, the release of growth factors can be sufficient to stimulate an angiogenic response that is maintained by the host tissue (H.-J. Cho et al., 2007). In our results, both Glo1 and WT BMC treatments resulted in a greater number of capillaries compared to PBS, yet no significant differences were detected between cell treatments. On the contrary, the angiogenesis study *in vitro* did show that Glo1 overexpression in BMCs could preserve their angiogenic potential and ability to incorporate into the cell network after exposure to MG compared to WT BMCs. In a previous study from our lab (Blackburn et al., 2017), c-kit$^+$ cells, a population from the bone marrow, were greatly incorporated into the hearts of infarcted Glo1 mice compared to the WT group. Importantly, BMCs isolated with the same protocol used in this study have been shown to be comprised of almost 30% of c-kit$^+$ cells (Vulesevic et al., 2014). These results are supported by the literature which indicates that the regeneration of blood vessels involves the mobilization of pro-angiogenic cells that are both local and bone marrow-derived. Their capacity to repair the vasculature is partly through direct participation in the formation of blood vessels, but mainly by releasing pro-angiogenic cytokines

that recruit local angiogenic cells (Fadini Gian et al., 2012). It has even been reported that conditioned media injected into infarcted hearts could have the same effect as cell transplantation (Timmers et al., 2011). For these reasons, we also analyzed the potential of conditioned media from ±MG-treated WT and Glo1 BMC to induce endothelial cell migration *in vitro*, however, no significant difference was found between the groups. A study that evaluated the migration and angiogenesis of endothelial cells exposed to MG reported that MG effect is dose-dependent and only concentrations of 25-100μM negatively affected migration (Liu et al., 2012). This suggests that the MG concentration used in the *in vitro* tests may be an important limitation in our results, as described later. Although the formation of new vessels in the affected area is critical for the healing process (Zymek et al., 2006) and our study demonstrated a superiority of BMCs compared to PBS, this was not enough to reduce the size of the infarct or to improve the cardiac function after MI.

Another consideration to our therapeutic approach is that, even if Glo1 is overexpressed, the depletion of GSH caused by oxidative stress (Thornalley, 2003) could limit the activity of Glo1 since it depends on GSH availability (Shinohara et al., 1998). Notably, GSH has been shown to be depleted due to culture conditions and common protocols, such as the trypsinization process (Bishop et al., 1985; Reiners et al., 2000). It might be convenient to replenish the cells with GSH before and during delivery of cell treatment so that Glo1 can function at its fullest. In addition to Glo1, activity of other protective enzymes such as SOD, catalase and glutathione peroxidase are reduced after MI (Hill & Singal, 1997). For this reason, aiming at reduction of one molecule alone may be insufficient to neutralize its deleterious effects in MI. A similar outcome was reported by another studies in which SOD was overexpressed to neutralize ROS, and the results were mixed (Bolli, 1988). Another study used an antioxidant therapy and reported that

association between ROS and heart disease is too complex to be addressable by a single intervention (Mak & Newton, 2004).

Since oxidative stress plays an important role in the progression of cardiac remodelling and dysfunction after MI (Kinugawa et al., 2000), two *in vitro* studies were conducted to determine the ability of Glo1 overexpression to decrease oxidative stress. Although the ROS assay showed that Glo1 BMCs produce significantly less ROS than their WT counterpart after exposure to MG, the results were admittedly confusing. In the first place, the fluorescence readings from wells with no cells (which consisted of fibronectin-coated wells with media and reagent kit) showed values as high as some readings with cells. This resulted in experimental values converting into negative numbers upon normalization (done by subtracting experimental values minus the value from the well with no cells). However, all treatments were performed under the same conditions and readings were made at the same time; and for this reason, pre-normalization results were shown instead. Secondly, WT BMCs exposed to PBS produced higher ROS levels than with MG and H_2O_2 exposure, which in theory should induce more ROS formation. These results also comprised a high variability between samples. In an attempt to better understand these results, two studies using the same number of cells ($4x10^4$) exposed to different concentrations of H_2O_2 (0μM, 1μM, 10μM, 100μM and 1mM) (Appendix: Figure 9.1A) and another study including different cell numbers ($0.1x10^4$, $2x10^4$, $4 x10^4$) exposed to the same concentration of 10μM H_2O_2 (Appendix, Figure 9.1B) were performed. Surprisingly, ROS levels were indirectly proportional to the number of cells, and the well without cells or H_2O_2 showed the same fluorescence as the well with the highest concentration of H_2O_2 (1 mM). For these reasons, the results of this assay should be interpreted with caution. The second test measured SOD production, one of the enzymes that scavenge ROS (Giordano, 2005) that has been shown

to be dysfunctional in post-ischemic conditions (Bolli, 1988). Only Glo1 BMCs exposed to PBS showed SOD production whereas all other cell groups exposed to MG or PBS exhibited negative values. This suggested that oxidative stress might originate intrinsically by the cell isolation protocols and cell culture conditions, as reported by others (Bishop et al., 1985; Halliwell, 2003) – regardless of MG addition. Under these circumstances, extra O_2^- would be available to react with the dye, resulting in absorbance values that fall outside the detectable limits by the kit. To facilitate the interpretation of results, the data was presented as availability of O_2^- to produce colorimetric reaction, which demonstrated that Glo1 BMCs can scavenge O_2^- more efficiently. Since studies have linked intracellular ROS increase with MG accumulation (Ceradini et al., 2008) and ROS has been shown to limit the survival of transplanted cells (Li et al., 2016), the reduction of oxidative stress found by Glo1 overexpression might confer protection to cells that aim to be used as a therapeutic option.

As mentioned above, the MG concentration used in this study to compare Glo1 BMCs vs. WT BMCs *in vitro* might have been a major limitation. Aiming to use the physiological MG levels found in cells after MI this study used as base the typical MG concentration of 1-4μM (Rabbani et al., 2016; Thornalley, 2008) and then added the 56% increase reported at 6h-post MI (Blackburn et al., 2017). Therefore, "abnormal concentrations" could be established within the range of 1.56 - 6.24 μM. In addition, the concentration of 5μM was previously used in our laboratory (Vulesevic et al., 2014) and falls within a range that has been reported by others (Chang et al., 2005). However, many studies that have reported toxic effects of MG in cell cultures have used concentrations as high as 100μM to 10mM (Chang et al., 2005). Although these concentrations have shown negative effects, they are unlikely to be of physiological relevance (Rabbani & Thornalley, 2008). Further complicating the issue is that measuring the

MG concentration in physiological systems has been a continuing problem due to the different routes through which it can be produced, artifacts that can manifest during the sample processing (Thornalley, 2008; Wang et al., 2010) and the use of different measuring methods (Chang et al., 2005). In addition, cell media constituents, cell type and cell culture age all variably promote the formation of oxidative stress (Bishop et al., 1985; Halliwell, 2003) thus affecting their vulnerability to MG effects and making direct comparisons challenging.

7. Future work

To date there is a great discrepancy as to which is the optimal concentration of MG to be used in *in vitro* testing and, on top of that, most of the studies reported have been performed in diabetes models (Wang et al., 2010). To ensure that the *in vitro* studies have greater physiological significance, future work could focus on quantifying the cellular and plasma levels of MG in the infarct and peri-infarct zones in MI models. Furthermore, future studies should contemplate that MG effects *in vivo* are often aggravated by its accumulation. Therefore, exposure to relatively low concentrations such as the one used in this study (5μM) might not reflect the effects of long-term accumulation; for this reason, MG concentrations of 10μM or 20μM could be used instead to test the effect of MG on BMC robustness.

For *in vivo* studies, future work could aim at increasing the number of BMCs injected (e.g. up to $1x10^6$ cells) (J. Cho et al., 2011; Duan et al., 2003; L. Li et al., 2013) so that results may be more comparable to those from other studies. Moreover, biomaterials could be combined with BMCs to increase the retention after transplantation and demonstrate the true potential of Glo1 overexpression. Since GSH is depleted by oxidative stress (Thornalley, 2003), future work could also consider replenishing Glo1 BMCs with GSH after harvesting/before injection and use them

as a combined therapy. To this end, biomaterials such as GSH-enriched microcapsules could be used to increase the therapeutic benefit of Glo1 BMCs. Then, additional experimentation might be required to establish if encapsulation can further protect transplanted cells from the MG that accumulates in the heart post-MI.

8. Conclusions

With CVDs as the leading cause of death worldwide and the lack of an effective treatment for severe MI, cell therapy offers a promising therapeutic approach to treat MI with the hopes of limiting cardiac remodeling and promoting myocardial repair/regeneration. While its potential has been demonstrated in both animal models and clinical trials, the benefits associated remain modest at best. Low cell viability and poor engraftment are two factors challenging this therapeutic approach. For this reason, this thesis aimed to evaluate, *in vitro* and *in vivo*, the ability of Glo1 overexpression to mitigate the negative effects of MG on BMC function, thus improving their efficacy as a therapy for MI.

A major contribution of this thesis is the finding that Glo1 expression is reduced early after MI at 2 days and this reduction persists for up to at least 14 days. The lowest level of expression was observed at 7 days post-MI, a timepoint that coincides to the proliferation stage of cardiac healing. Our *in vitro* results suggested preservation in the function of Glo1-overexpressing cells after exposure to MG that was not observed on their WT counterpart in terms of greater angiogenic potential and reduced ROS production. However, no difference was found between WT and Glo1 BMCs exposed to MG in terms of viability, migration and SOD production *in vitro*. *In vivo*, hearts treated with PBS, WT or Glo1 BMCs showed no difference in cardiac function or scar formation. However, infarcted hearts treated with BMCs yielded higher number of

capillaries in the border zone than those treated with PBS. Importantly, at 21 days after injection, donor cells were not detected in the hearts of the recipients, suggesting the lack of long-term retention as a possible explanation as to why no significant improvement was shown by Glo1 BMCs. Overall, based on these results we conclude that overexpression of Glo1 in BMCs does not confer superior therapeutic potential under the conditions tested.

9. Appendix

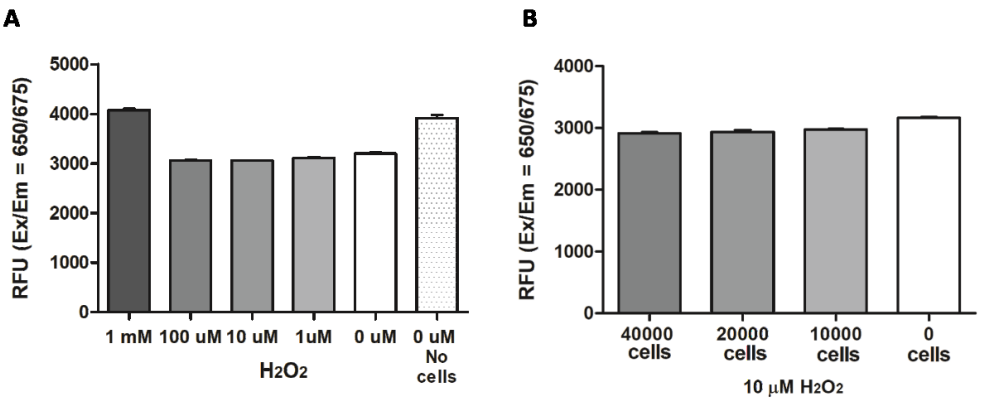

Figure 9.1. ROS assay - the troubleshooting. To evaluate the reliability of the ROS assay results, an assay using different H_2O_2 concentration with same number of cells **(A)**, as well as an assay varying the number of cells exposed to a stable concentration of H_2O_2 **(B)** were carried out. Each condition (n=2) was exposed to H_2O_2 for 30 mins/37°C prior to exposure to ROS assay reagents and reading Ex/Em=650/675. Data expressed in relative fluorescence units (RFU).

10. References

Abordo, E. A., Minhas, H. S., & Thornalley, P. J. (1999). Accumulation of alpha-oxoaldehydes during oxidative stress: a role in cytotoxicity. *Biochemical Pharmacology*, *58*(4), 641–648.

Ahmed, U., Dobler, D., Larkin, S. J., Rabbani, N., & Thornalley, P. J. (2008). Reversal of

hyperglycemia-induced angiogenesis deficit of human endothelial cells by overexpression of glyoxalase 1 in vitro. *Annals of the New York Academy of Sciences*, *1126*, 262–264. https://doi.org/10.1196/annals.1433.035

Aleshin, A., Ananthakrishnan, R., Li, Q., Rosario, R., Lu, Y., Qu, W., … Ramasamy, R. (2008). RAGE modulates myocardial injury consequent to LAD infarction via impact on JNK and STAT signaling in a murine model. *American Journal of Physiology-Heart and Circulatory Physiology*, *294*(4), H1823–H1832. https://doi.org/10.1152/ajpheart.01210.2007

Arnous, S., Mozid, A., Martin, J., & Mathur, A. (2012). Bone marrow mononuclear cells and acute myocardial infarction. *Stem Cell Research & Therapy*, *3*(1), 2. https://doi.org/10.1186/scrt93

Benavides-Vallve, C., Corbacho, D., Iglesias-Garcia, O., Pelacho, B., Albiasu, E., Castaño, S., … Ortiz-de-Solorzano, C. (2012). New Strategies for Echocardiographic Evaluation of Left Ventricular Function in a Mouse Model of Long-Term Myocardial Infarction. *PLoS ONE*, *7*(7), e41691. https://doi.org/10.1371/journal.pone.0041691

Benjamin, E. J., Blaha, M. J., Chiuve, S. E., Cushman, M., Das, S. R., Deo, R., … Muntner, P. (2017). Heart Disease and Stroke Statistics-2017 Update: A Report From the American Heart Association. *Circulation*, *135*(10), e146–e603. https://doi.org/10.1161/CIR.0000000000000485

Berner, A. K., Brouwers, O., Pringle, R., Klaassen, I., Colhoun, L., McVicar, C., … Stitt, A. W. (2012). Protection against methylglyoxal-derived AGEs by regulation of glyoxalase 1 prevents retinal neuroglial and vasodegenerative pathology. *Diabetologia*, *55*(3), 845–854. https://doi.org/10.1007/s00125-011-2393-0

Bishop, C., Mirza, Z., Crapo, J., & Freeman, B. (1985). Free radical damage to cultured porcine aortic endothelial cells and lung fibroblasts: Modulation by culture conditions. *In Vitro Cellular & Developmental Biology*, *21*(4), 229–236. https://doi.org/10.1007/BF02620934

Blackburn, N., Vulesevic, B., McNeill, B., Cimenci, C., Ahmadi, A., Gonzalez-Gomez, M., … Suuronen, E. (2017). Methylglyoxal-derived advanced glycation end products contribute to negative cardiac remodeling and dysfunction post-myocardial infarction. *Basic Research in*

Cardiology, *112*(5), 1–14. https://doi.org/10.1007/s00395-017-0646-x

Bolli, R. (1988). Oxygen-derived free radicals and postischemic myocardial dysfunction ("stunned myocardium"). *Journal of the American College of Cardiology*, *12*(1), 239–249.

Braunwald, E. (1997). Cardiovascular medicine at the turn of the millennium: triumphs, concerns, and opportunities. *N Engl J Med*, *337*.

Brouwers, O., Niessen, P. M., Ferreira, I., Miyata, T., Scheffer, P. G., Teerlink, T., … Schalkwijk, C. G. (2011). Overexpression of glyoxalase-I reduces hyperglycemia-induced levels of advanced glycation end products and oxidative stress in diabetic rats. *The Journal of Biological Chemistry*, *286*(2), 1374–1380. https://doi.org/10.1074/jbc.M110.144097

Brouwers, O., Yu, L., Niessen, P., Slenter, J., Jaspers, K., Wagenaar, A., … Schalkwijk, C. (2016). Glyoxalase-1 overexpression partially prevents diabetes-induced impaired arteriogenesis in a rat hindlimb ligation model. *Glycoconjugate Journal*, *33*(4), 627–630. https://doi.org/10.1007/s10719-016-9681-3

Bucciarelli, L. G., Kaneko, M., Ananthakrishnan, R., Harja, E., Lee, L. K., Hwang, Y. C., … Ramasamy, R. (2006). Receptor for Advanced-Glycation End Products. *Circulation*, *113*(9), 1226 LP-1234. Retrieved from http://circ.ahajournals.org/content/113/9/1226.abstract

Burke, A. P., & Virmani, R. (2007). Pathophysiology of Acute Myocardial Infarction. *Medical Clinics of North America*, *91*(4), 553–572. https://doi.org/https://doi.org/10.1016/j.mcna.2007.03.005

Ceradini, D. J., Yao, D., Grogan, R. H., Callaghan, M. J., Edelstein, D., Brownlee, M., & Gurtner, G. C. (2008). Decreasing Intracellular Superoxide Corrects Defective Ischemia-induced New Vessel Formation in Diabetic Mice. *The Journal of Biological Chemistry*, *283*(16), 10930–10938. https://doi.org/10.1074/jbc.M707451200

Chang, T., Wang, R., & Wu, L. (2005). Methylglyoxal-induced nitric oxide and peroxynitrite production in vascular smooth muscle cells. *Free Radical Biology and Medicine*, *38*(2), 286–293. https://doi.org/https://doi.org/10.1016/j.freeradbiomed.2004.10.034

Chen, W., & Frangogiannis, N. G. (2013). Fibroblasts in post-infarction inflammation and cardiac repair. *Biochimica et Biophysica Acta (BBA) - Molecular Cell Research*, *1833*(4), 945–953.

https://doi.org/https://doi.org/10.1016/j.bbamcr.2012.08.023

Cho, H.-J., Lee, N., Lee, J. Y., Choi, Y. J., Ii, M., Wecker, A., … Yoon, Y. (2007). Role of host tissues for sustained humoral effects after endothelial progenitor cell transplantation into the ischemic heart. *The Journal of Experimental Medicine*, *204*(13), 3257–3269. https://doi.org/10.1084/jem.20070166

Cho, J., Zhai, P., Maejima, Y., & Sadoshima, J. (2011). Myocardial injection with GSK-3beta-overexpressing bone marrow-derived mesenchymal stem cells attenuates cardiac dysfunction after myocardial infarction. *Circulation Research*, *108*(4), 478–489. https://doi.org/10.1161/CIRCRESAHA.110.229658

Dewald, O., Zymek, P., Winkelmann, K., Koerting, A., Ren, G., Abou-Khamis, T., … Frangogiannis, N. G. (2005). CCL2/Monocyte Chemoattractant Protein-1 regulates inflammatory responses critical to healing myocardial infarcts. *Circulation Research*, *96*(8), 881–889. https://doi.org/10.1161/01.RES.0000163017.13772.3a

Dobaczewski, M., Gonzalez-Quesada, C., & Frangogiannis, N. G. (2010). The extracellular matrix as a modulator of the inflammatory and reparative response following myocardial infarction. *Journal of Molecular and Cellular Cardiology*, *48*(3), 504–511. https://doi.org/10.1016/j.yjmcc.2009.07.015

Dobler, D., Ahmed, N., Song, L., Eboigbodin, K. E., & Thornalley, P. J. B. T.-D. (2006). Increased dicarbonyl metabolism in endothelial cells in hyperglycemia induces anoikis and impairs angiogenesis by RGD and GFOGER motif modification, *55*(7), 1961+. Retrieved from http://link.galegroup.com.proxy.bib.uottawa.ca/apps/doc/A148481483/AONE?u=otta77973&sid=AONE&xid=30ab8020

Duan, H.-F., Wu, C.-T., Wu, D.-L., Lu, Y., Liu, H.-J., Ha, X.-Q., … Wang, L.-S. (2003). Treatment of myocardial ischemia with bone marrow-derived mesenchymal stem cells overexpressing hepatocyte growth factor. *Molecular Therapy : The Journal of the American Society of Gene Therapy*, *8*(3), 467–474.

Fadini Gian, P., Losordo Douglas, P., & Dimmeler Stefanie, P. (2012). Critical Reevaluation of Endothelial Progenitor Cell Phenotypes for Therapeutic and Diagnostic Use. *Circulation*

Research, *110*(4), 624–637. https://doi.org/10.1161/CIRCRESAHA.111.243386

Fazel, S., Cimini, M., Chen, L., Li, S., Angoulvant, D., Fedak, P., … Li, R.-K. (2006). Cardioprotective [c-kit.sup.+] cells are from the bone marrow and regulate the myocardial balance of angiogenic cytokines.(medical research)(includes statistical table). *Journal of Clinical Investigation*, *116*(7), 1865. https://doi.org/10.1172/JCI27019

Ferrari, R., Ceconi, C., Curello, S., Guarnieri, C., Caldarera, C. M., Albertini, A., & Visioli, O. (1985). Oxygen-mediated myocardial damage during ischameia and reperfusion: Role of the cellular defences against oxygen toxicity. *Journal of Molecular and Cellular Cardiology*, *17*(10), 937–945. https://doi.org/https://doi.org/10.1016/S0022-2828(85)80074-2

Frangogiannis, N. G. (2006). The mechanistic basis of infarct healing. *Antioxidants & Redox Signaling*, *8*(11–12), 1907–1939. https://doi.org/10.1089/ars.2006.8.1907

Frangogiannis, N. G. (2014). The inflammatory response in myocardial injury, repair and remodeling. *Nature Reviews. Cardiology*, *11*(5), 255–265. https://doi.org/10.1038/nrcardio.2014.28

Geissmann, F., Manz, M. G., Jung, S., Sieweke, M. H., Merad, M., & Ley, K. (2010). Development of monocytes, macrophages, and dendritic cells. *Science (New York, N.Y.)*, *327*(5966), 656–661. https://doi.org/10.1126/science.1178331

Giordano, F. J. (2005). Oxygen, oxidative stress, hypoxia, and heart failure. *Journal of Clinical Investigation*, *115*(3), 500–508. https://doi.org/10.1172/JCI200524408

Guzy, R. D., Hoyos, B., Robin, E., Chen, H., Liu, L., Mansfield, K. D., … Schumacker, P. T. (2005). Mitochondrial complex III is required for hypoxia-induced ROS production and cellular oxygen sensing. *Cell Metabolism*, *1*(6), 401–408. https://doi.org/https://doi.org/10.1016/j.cmet.2005.05.001

Halliwell, B. (2003). Oxidative stress in cell culture: an under-appreciated problem? *FEBS Letters*, *540*(1–3), 3–6. https://doi.org/10.1016/S0014-5793(03)00235-7

Hanssen, N. M. J., Scheijen, J. L. J. M., Jorsal, A., Parving, H.-H., Tarnow, L., Rossing, P., … Schalkwijk, C. G. (2017). Higher Plasma Methylglyoxal Levels Are Associated With Incident Cardiovascular Disease in Individuals With Type 1 Diabetes: A 12-Year Follow-up Study.

Diabetes, *66*(8), 2278–2283. https://doi.org/10.2337/db16-1578

Hanssen, N. M. J., Westerink, J., Scheijen, J. L. J. M., van der Graaf, Y., Stehouwer, C. D. A., & Schalkwijk, C. G. (2018). Higher Plasma Methylglyoxal Levels Are Associated With Incident Cardiovascular Disease and Mortality in Individuals With Type 2 Diabetes. *Diabetes Care*. Retrieved from http://care.diabetesjournals.org/content/early/2018/05/18/dc18-0159.abstract

Hanssen, N. M. J., Wouters, K., Huijberts, M. S., Gijbels, M. J., Sluimer, J. C., Scheijen, J. L. J. M., … Schalkwijk, C. G. (2014). Higher levels of advanced glycation endproducts in human carotid atherosclerotic plaques are associated with a rupture-prone phenotype. *European Heart Journal*, *35*(17), 1137–1146. Retrieved from http://dx.doi.org/10.1093/eurheartj/eht402

Hill, M. F., & Singal, P. K. (1997). Right and left myocardial antioxidant responses during heart failure subsequent to myocardial infarction. *Circulation*, *96*(7), 2414–2420.

Hodgkinson, C. P., Bareja, A., Gomez, J. A., & Dzau, V. J. (2016). Emerging Concepts in Paracrine Mechanisms in Regenerative Cardiovascular Medicine and Biology. *Circulation Research*, *118*(1), 95 LP-107. Retrieved from http://circres.ahajournals.org/content/118/1/95.abstract

Kalra, B. S., & Roy, V. (2012). Efficacy of Metabolic Modulators in Ischemic Heart Disease. *The Journal of Clinical Pharmacology*, *52*(3), 292–305. https://doi.org/10.1177/0091270010396042

Kanda, P., & Davis, D. R. (2017). Cellular mechanisms underlying cardiac engraftment of stem cells. *Expert Opinion on Biological Therapy*. Taylor & Francis. https://doi.org/10.1080/14712598.2017.1346080

Kandaswamy, E., & Zuo, L. (2018). Recent Advances in Treatment of Coronary Artery Disease: Role of Science and Technology. *International Journal of Molecular Sciences*, *19*(2). https://doi.org/10.3390/ijms19020424

Kanno, S., Lerner, D. L., Schuessler, R. B., Betsuyaku, T., Yamada, K. A., Saffitz, J. E., & Kovacs, A. (2002). Echocardiographic evaluation of ventricular remodeling in a mouse model of myocardial infarction. *Journal of the American Society of Echocardiography : Official*

Publication of the American Society of Echocardiography, *15*(6), 601–609.

Kinugawa, S., Tsutsui, H., Hayashidani, S., Ide, T., Suematsu, N., Satoh, S., … Takeshita, A. (2000). Treatment with dimethylthiourea prevents left ventricular remodeling and failure after experimental myocardial infarction in mice: role of oxidative stress. *Circulation Research*, *87*(5), 392–398.

Kwon, Y.-W., Yang, H.-M., & Cho, H.-J. (2010). Cell Therapy for Myocardial Infarction. *International Journal of Stem Cells*, *3*(1), 8–15. Retrieved from http://www.ncbi.nlm.nih.gov/pmc/articles/PMC4022684/

Laflamme, M. A., & Murry, C. E. (2011). Heart Regeneration. *Nature*, *473*(7347), 326–335. https://doi.org/10.1038/nature10147

Lemcke, H., Voronina, N., Steinhoff, G., & David, R. (2018). Recent Progress in Stem Cell Modification for Cardiac Regeneration. *Stem Cells International*, *2018*, 1909346. https://doi.org/10.1155/2018/1909346

Lesnefsky, E. J., & Hoppel, C. L. (2003). Ischemia–reperfusion injury in the aged heart: role of mitochondria. *Archives of Biochemistry and Biophysics*, *420*(2), 287–297. https://doi.org/https://doi.org/10.1016/j.abb.2003.09.046

Li, J.-R., & Qu, T.-T. (2017). Into the eyes of bone marrow-derived mesenchymal stem cells therapy for myocardial infarction and other diseases. *Stem Cell Investigation*, *4*(8), 69. https://doi.org/10.21037/sci.2017.08.01

Li, L., Zeng, H., Hou, X., He, X., & Chen, J.-X. (2013). Myocardial injection of apelin-overexpressing bone marrow cells improves cardiac repair via upregulation of Sirt3 after myocardial infarction. *PLoS ONE*, *8*(9), e71041. https://doi.org/10.1371/journal.pone.0071041

Li, X., Tamama, K., Xie, X., & Guan, J. (2016). Improving Cell Engraftment in Cardiac Stem Cell Therapy. *Stem Cells International*, *2016*, 7168797. https://doi.org/10.1155/2016/7168797

Liu, H., Yu, S., Zhang, H., & Xu, J. (2012). Angiogenesis impairment in diabetes: role of methylglyoxal-induced receptor for advanced glycation endproducts, autophagy and vascular endothelial growth factor receptor 2. *PloS One*, *7*(10), e46720.

https://doi.org/10.1371/journal.pone.0046720

Mak, S., & Newton, G. E. (2004). Redox modulation of the inotropic response to dobutamine is impaired in patients with heart failure. *American Journal of Physiology. Heart and Circulatory Physiology*, *286*(2), H789-95. https://doi.org/10.1152/ajpheart.00633.2003

Mangi, A. A., Noiseux, N., Kong, D., He, H., Rezvani, M., Ingwall, J. S., & Dzau, V. J. (2003). Mesenchymal stem cells modified with Akt prevent remodeling and restore performance of infarcted hearts. *Nature Medicine*, *9*(9), 1195–1201. https://doi.org/10.1038/nm912

Mathur, A., Arnold, R., Assmus, B., Bartunek, J., Belmans, A., Bönig, H., … Zeiher, A. (2017). The effect of intracoronary infusion of bone marrow-derived mononuclear cells on all-cause mortality in acute myocardial infarction: rationale and design of the BAMI trial. *European Journal of Heart Failure*, *19*(11), 1545–1550. https://doi.org/10.1002/ejhf.829

Matsui, Y., Morimoto, J., & Uede, T. (2010). Role of matricellular proteins in cardiac tissue remodeling after myocardial infarction. *World Journal of Biological Chemistry*, *1*(5), 69–80. https://doi.org/10.4331/wjbc.v1.i5.69

Mayfield, A. E., Tilokee, E. L., Latham, N., Mcneill, B., Lam, B.-K., Ruel, M., … Davis, D. R. (2014). The effect of encapsulation of cardiac stem cells within matrix-enriched hydrogel capsules on cell survival, post-ischemic cell retention and cardiac function. *Biomaterials*, *35*(1), 133–142. https://doi.org/10.1016/j.biomaterials.2013.09.085

Murry, C. E., Reinecke, H., & Pabon, L. M. (2006). Regeneration gaps: observations on stem cells and cardiac repair. *Journal of the American College of Cardiology*, *47*(9), 1777–1785. https://doi.org/10.1016/j.jacc.2006.02.002

Musialek, P., Tekieli, L., Kostkiewicz, M., Miszalski-Jamka, T., Klimeczek, P., Mazur, W., … Wojakowski, W. (2013). Infarct size determines myocardial uptake of CD34+ cells in the peri-infarct zone: results from a study of (99m)Tc-extametazime-labeled cell visualization integrated with cardiac magnetic resonance infarct imaging. *Circulation. Cardiovascular Imaging*, *6*(2), 320–328. https://doi.org/10.1161/CIRCIMAGING.112.979633

Nah, D.-Y., & Rhee, M.-Y. (2009). The Inflammatory Response and Cardiac Repair After Myocardial Infarction. *Korean Circulation Journal*, *39*(10), 393–398.

https://doi.org/10.4070/kcj.2009.39.10.393

Nahrendorf, M., Pittet, M. J., & Swirski, F. K. (2010). Monocytes: protagonists of infarct inflammation and repair after myocardial infarction. *Circulation*, *121*(22), 2437–2445. https://doi.org/10.1161/CIRCULATIONAHA.109.916346

Orlic, D., Kajstrua, J., & Chimenti, S. (2001). Bone marrow cells regenerate infarcted myocardium. *Nature*, *410*.

Prabhu, S. D., & Frangogiannis, N. G. (2016). The Biological Basis for Cardiac Repair After Myocardial Infarction: From Inflammation to Fibrosis. *Circulation Research*, *119*(1), 91–112. https://doi.org/10.1161/CIRCRESAHA.116.303577

Public Health Agency of Canada. (2017). *Heart disease in Canada: Highlights from the Canadian Chronic Disease Surveillance System*. Ottawa, ON. https://doi.org/ISBN: HP35-85/2017E-PDF

Rabbani, N., & Thornalley, P. J. (2008). Dicarbonyls linked to damage in the powerhouse: glycation of mitochondrial proteins and oxidative stress. *Biochemical Society Transactions*, *36*(Pt 5), 1045–1050. https://doi.org/10.1042/BST0361045

Rabbani, N., Xue, M., & Thornalley, P. J. (2016). Methylglyoxal-induced dicarbonyl stress in aging and disease: first steps towards glyoxalase 1-based treatments. *Clinical Science*, *130*(19), 1677 LP-1696. Retrieved from http://www.clinsci.org/content/130/19/1677.abstract

Rane, A. A., & Christman, K. L. (2011). Biomaterials for the Treatment of Myocardial Infarction: A 5-Year Update. *Journal of the American College of Cardiology*, *58*(25), 2615–2629. https://doi.org/https://doi.org/10.1016/j.jacc.2011.11.001

Reed, G. W., Rossi, J. E., & Cannon, C. P. (2017). Acute myocardial infarction. *The Lancet*. https://doi.org/10.1016/S0140-6736(16)30677-8

Reiners, J. J., Mathieu, P., Okafor, C., Putt, D. A., & Lash, L. H. (2000). Depletion of cellular glutathione by conditions used for the passaging of adherent cultured cells. *Toxicology Letters*, *115*(2), 153–163. https://doi.org/https://doi.org/10.1016/S0378-4274(00)00189-2

Rosca, M. G., Mustata, T. G., Kinter, M. T., Ozdemir, A. M., Kern, T. S., Szweda, L. I., … Weiss, M.

F. (2005). Glycation of mitochondrial proteins from diabetic rat kidney is associated with excess superoxide formation. *American Journal of Physiology. Renal Physiology*, *289*(2), F420-30. https://doi.org/10.1152/ajprenal.00415.2004

Schalkwijk, C. G. (2015). Vascular AGE-ing by methylglyoxal: the past, the present and the future. *Diabetologia*, *58*(8), 1715–1719. https://doi.org/10.1007/s00125-015-3597-5

Shinohara, M., Thornalley, P. J., Giardino, I., Beisswenger, P., Thorpe, S. R., Onorato, J., & Brownlee, M. (1998). Overexpression of glyoxalase-I in bovine endothelial cells inhibits intracellular advanced glycation endproduct formation and prevents hyperglycemia-induced increases in macromolecular endocytosis. *The Journal of Clinical Investigation*, *101*(5), 1142–1147. https://doi.org/10.1172/JCI119885

Singh, A., Singh, A., & Sen, D. (2016). Mesenchymal stem cells in cardiac regeneration: a detailed progress report of the last 6 years (2010-2015). *Stem Cell Research & Therapy*, *7*(1). https://doi.org/10.1186/s13287-016-0341-0

Sun, Y. (2009). Myocardial repair/remodelling following infarction: roles of local factors. *Cardiovascular Research*, *81*(3), 482–490. https://doi.org/10.1093/cvr/cvn333

Takagawa, J., Zhang, Y., Wong, M. L., Sievers, R. E., Kapasi, N. K., Wang, Y., … Springer, M. L. (2007). Myocardial Infarct Size Measurement in the Mouse Chronic Infarction Model: Comparison of Area- and Length-Based Approaches. *Journal of Applied Physiology (Bethesda, Md. : 1985)*, *102*(6), 2104–2111. https://doi.org/10.1152/japplphysiol.00033.2007

Thornalley, P. J. (1998). Cell activation by glycated proteins. AGE receptors, receptor recognition factors and functional classification of AGEs. *Cellular and Molecular Biology (Noisy-Le-Grand, France)*, *44*(7), 1013–1023.

Thornalley, P. J. (2003). Glyoxalase I--structure, function and a critical role in the enzymatic defence against glycation. *Biochemical Society Transactions*, *31*(Pt 6), 1343–1348. https://doi.org/10.1042/

Thornalley, P. J. (2004). Glycation, receptor-mediated cell activation and vascular complications of diabetes. *Diabetes & Vascular Disease Research*. https://doi.org/10.3132/dvdr.2004.002

Thornalley, P. J. (2008). Protein and nucleotide damage by glyoxal and methylglyoxal in physiological systems - role in ageing and disease. *Drug Metabolism and Drug Interactions*, *23*(1–2), 125–150. Retrieved from http://www.ncbi.nlm.nih.gov/pmc/articles/PMC2649415/

Thornalley, P. J., Strath, M., & Wilson, R. J. (1994). Antimalarial activity in vitro of the glyoxalase I inhibitor diester, S-p-bromobenzylglutathione diethyl ester. *Biochemical Pharmacology*, *47*(2), 418. https://doi.org/10.1016/0006-2952(94)90035-3

Thygesen, K., Alpert, J. S., Jaffe, A. S., Simoons, M. L., Chaitman, B. R., & White, H. D. (2012). Third Universal Definition of Myocardial Infarction. *Circulation*, *126*(16), 2020 LP-2035. Retrieved from http://circ.ahajournals.org/content/126/16/2020.abstract

Timmers, L., Lim, S. K., Hoefer, I. E., Arslan, F., Lai, R. C., van Oorschot, A. A. M., … de Kleijn, D. P. V. (2011). Human mesenchymal stem cell-conditioned medium improves cardiac function following myocardial infarction. *Stem Cell Research*, *6*(3), 206–214. https://doi.org/https://doi.org/10.1016/j.scr.2011.01.001

Vanden Hoek, T. L., Li, C., Shao, Z., Schumacker, P. T., & Becker, L. B. (1997). Significant Levels of Oxidants are Generated by Isolated Cardiomyocytes During Ischemia Prior to Reperfusion. *Journal of Molecular and Cellular Cardiology*, *29*(9), 2571–2583. https://doi.org/https://doi.org/10.1006/jmcc.1997.0497

Vulesevic, B., McNeill, B., Geoffrion, M., Kuraitis, D., McBane, J. E., Lochhead, M., … Suuronen, E. J. (2014). Glyoxalase-1 overexpression in bone marrow cells reverses defective neovascularization in STZ-induced diabetic mice. *Cardiovascular Research*, *101*(2), 306–316. https://doi.org/10.1093/cvr/cvt259

Vulesevic, B., McNeill, B., Giacco, F., Maeda, K., Blackburn, N. J. R., Brownlee, M., … Suuronen, E. J. (2016). Methylglyoxal-Induced Endothelial Cell Loss and Inflammation Contribute to the Development of Diabetic Cardiomyopathy. *Diabetes*, *65*(6), 1699–1713. https://doi.org/10.2337/db15-0568

Wang, X.-L., Lau, W. B., Yuan, Y.-X., Wang, Y.-J., Yi, W., Christopher, T. A., … Ma, X.-L. (2010). Methylglyoxal increases cardiomyocyte ischemia-reperfusion injury via glycative inhibition

of thioredoxin activity. *American Journal of Physiology - Endocrinology and Metabolism*, *299*(2), E207–E214. https://doi.org/10.1152/ajpendo.00215.2010

Ward, M. R., Connelly, K. A., Vijayaraghavan, R., Vaags, A. K., Graham, J. J., Foltz, W., … Dick, A. (2013). eNOS overexpressing bone marrow cells are safe and effective in a porcine model of myocardial regeneration following acute myocardial infarction. *Cardiovascular Therapeutics*, *31*(6), e72-8. https://doi.org/10.1111/1755-5922.12037

Weintraub, W. S., Daniels, S. R., Burke, L. E., Franklin, B. A., Goff, D. C., Hayman, L. L., … Whitsel, L. P. (2011). Value of Primordial and Primary Prevention for Cardiovascular Disease. *Circulation*, *124*(8), 967 LP-990. Retrieved from http://circ.ahajournals.org/content/124/8/967.abstract

Yan, X., Anzai, A., Katsumata, Y., Matsuhashi, T., Ito, K., Endo, J., … Sano, M. (2013). Temporal dynamics of cardiac immune cell accumulation following acute myocardial infarction. *Journal of Molecular and Cellular Cardiology*, *62*, 24–35. https://doi.org/10.1016/j.yjmcc.2013.04.023

Zeisberg, E. M., Tarnavski, O., Zeisberg, M., Dorfman, A. L., McMullen, J. R., Gustafsson, E., … Kalluri, R. (2007). Endothelial-to-mesenchymal transition contributes to cardiac fibrosis. *Nature Medicine*, *13*(8), 952–961. https://doi.org/10.1038/nm1613

Zymek, P., Bujak, M., Chatila, K., Cieslak, A., Thakker, G., Entman, M. L., & Frangogiannis, N. G. (2006). The Role of Platelet-Derived Growth Factor Signaling in Healing Myocardial Infarcts. *Journal of the American College of Cardiology*, *48*(11), 2315–2323. https://doi.org/10.1016/j.jacc.2006.07.060